A CLIMATOLOGICAL STUDY OF THE FORCING OF THE NORTH PACIFIC OCEAN BY SYNOPTIC STORM ACTIVITY

Michael Scott Risch

NAVAL POSTGRADUATE SCHOOL
Monterey, California

THESIS

A CLIMATOLOGICAL STUDY OF THE FORCING OF THE NORTH PACIFIC OCEAN BY SYNOPTIC STORM ACTIVITY

by

Michael Scott Risch

March 1980

Thesis Advisor: R. L. Haney

SECURITY CLASSIFICATION OF THIS PAGE (When Data Entered)

REPORT DOCUMENTATION PAGE		READ INSTRUCTIONS BEFORE COMPLETING FORM
1. REPORT NUMBER	2. GOVT ACCESSION NO.	3. RECIPIENT'S CATALOG NUMBER
4. TITLE (and Subtitle) A Climatological Study of the Forcing of the North Pacific Ocean by Synoptic Storm Activity		5. TYPE OF REPORT & PERIOD COVERED Master's Thesis; March 1980 6. PERFORMING ORG. REPORT NUMBER
7. AUTHOR(s) Michael Scott Risch		8. CONTRACT OR GRANT NUMBER(s)
9. PERFORMING ORGANIZATION NAME AND ADDRESS Naval Postgraduate School Monterey, California 93940		10. PROGRAM ELEMENT, PROJECT, TASK AREA & WORK UNIT NUMBERS
11. CONTROLLING OFFICE NAME AND ADDRESS Naval Postgraduate School Monterey, California 93940		12. REPORT DATE March 1980 13. NUMBER OF PAGES 66
14. MONITORING AGENCY NAME & ADDRESS(if different from Controlling Office)		15. SECURITY CLASS. (of this report) Unclassified 15a. DECLASSIFICATION/DOWNGRADING SCHEDULE

16. DISTRIBUTION STATEMENT (of this Report)

Approved for public release; distribution unlimited.

17. DISTRIBUTION STATEMENT (of the abstract entered in Block 20, if different from Report)

18. SUPPLEMENTARY NOTES

19. KEY WORDS (Continue on reverse side if necessary and identify by block number)

NORPAX
Synoptic Storm Activity
SST Anomalies
Ocean Forcing

20. ABSTRACT (Continue on reverse side if necessary and identify by block number)

Synoptic storm activity over the North Pacific Ocean is investigated using a special series of six-hourly surface wind analyses prepared by Fleet Numerical Oceanographic Center (FNOC) covering the period 1969-1978. Temporal variance of the surface wind components at each grid point is "high pass" filtered, thereby removing all temporal variability

DD FORM 1 JAN 73 1473 EDITION OF 1 NOV 65 IS OBSOLETE
S/N 0102-014-6601

SECURITY CLASSIFICATION OF THIS PAGE (When Data Entered)

except that having time scales less than ten days. Both the total and the filtered wind components were used to calculate the cube of the friction velocity (u_*^3) and the wind stress curl ($curl_z \tau$).

Monthly "climatologies" are calculated by computing ten-year averages of monthly mean u_*^3 and $curl_z \tau$ from total and filtered wind components for each month of the year. It was found that while climatological maps of u_*^3 calculated from filtered data show spatially coherent patterns that are clearly associated with monthly storm tracks, similar maps of $curl_z \tau$ do not show such coherent patterns.

Maps of anomalous storm activity, as given by the difference between the monthly value and the climatological value for that month, are also prepared and qualitatively compared to observations of large scale sea surface temperature (SST) anomalies. Fairly good agreement is found between monthly mean u_*^3 anomalies calculated from the filtered data, and the observed development of SST anomalies during the winter of 1976-1977.

Approved for public release; distribution unlimited.

A Climatological Study of the Forcing of the North Pacific Ocean by Synoptic Storm Activity

by

Michael Scott Risch
Captain, United States Air Force
B.S., St. Louis University, 1972

Submitted in partial fulfillment of the
requirements for the degree of

MASTER OF SCIENCE IN METEOROLOGY

from the
NAVAL POSTGRADUATE SCHOOL
March 1980

ABSTRACT

Synoptic storm activity over the North Pacific Ocean is investigated using a special series of six-hourly surface wind analyses prepared by Fleet Numerical Oceanographic Center (FNOC) covering the period 1969-1978. Temporal variance of the surface wind components at each grid point is "high pass" filtered, thereby removing all temporal variability except that having time scales less than ten days. Both the total and the filtered wind components were used to calculate the cube of the friction velocity (u_*^3) and the wind stress curl ($curl_z \tau$).

Monthly "climatologies" are calculated by computing ten-year averages of monthly mean u_*^3 and $curl_z \tau$ from total and filtered wind components for each month of the year. It was found that while climatological maps of u_*^3 calculated from filtered data show spatially coherent patterns that are clearly associated with monthly storm tracks, similar maps of $curl_z \tau$ do not show such coherent patterns.

Maps of anomalous storm activity, as given by the difference between the monthly value and the climatological value for that month, are also prepared and qualitatively compared to observations of large scale sea surface temperature (SST) anomalies. Fairly good agreement is found between monthly mean u_*^3 anomalies calculated from the filtered data, and the observed development of SST anomalies during the winter of 1976-1977.

TABLE OF CONTENTS

LIST OF TABLES

LIST OF FIGURES

ACKNOWLEDGEMENTS

A great deal of gratitude and appreciation goes to Dr. Robert L. Haney for his guidance, patience, and friendship. Thanks are also due Dr. Russell L. Elsberry for his technical advice and Mr. Patrick C. Gallacher for his assistance in data handling. The author would like to recognize the professionalism of the staff of the W. R. Church Computer Center, specifically, Mr. Edwin V. Donellan, Ms. Jeanine M. Washington, Mr. Mannus Anderson and Ms. JoAnne H. Kallweit. Last but not least, if it were not for a loving wife and family all this would not have been possible.

I. INTRODUCTION

There have been many studies investigating the response of the upper ocean to strong atmospheric forcing events. By using many years of data from Ocean Weather Ships P, V, and N, Elsberry and Camp (1978) showed that a major fraction of the oceanic thermal structure modification during September to December is due to strong atmospheric forcing. An earlier study by Simpson (1969) suggests that synoptic scale disturbances control air-sea interaction over the extratropical oceans. The choice of an indicator of the atmospheric circulation has varied. Namias (1972 and 1978) worked with monthly mean 700 mb height fields while Davis (1976) worked with monthly mean sea-level pressure fields. In the latter study Davis used linear statistical predictors to examine connections between thermal variability in the North Pacific Ocean and variations in the state of the overlying atmosphere. He also suggests that atmospheric storminess may show a greater connection with sea surface temperature (SST) than does pressure. In a preceding thesis study, using 12-hourly data covering but a single year, Heise (1977) found that synoptic storms, or the lack of them, were related to anomalously cold, or warm, SST patterns. Heise was not, however, able to examine anomalous storm activity nor to compare it with SST anomalies.

The objective of this study has been to examine ten years of synoptic wind data for the purpose of describing synoptic storm activity. Using a series of six-hourly surface wind analyses prepared by Fleet Numerical Oceanographic Center (FNOC) covering the period 1969-1978, the temporal variance of the surface wind components at each individual grid point was "high-pass" filtered. The filter removed most of the temporal variability having time scales greater than ten days. Therefore, the circulation primarily due to moving synoptic storm systems was extracted from the total circulation.

Heise (1977) showed that filtered data does describe monthly mean storminess over a period of one year (1975) and that this storminess was qualitatively related to SST anomalies during that year. From both the filtered and unfiltered wind data, Heise (1977) computed the vertical component of the curl of the wind stress ($curl_z \tau$) and the friction velocity cubed (u_*^3). These quantities were selected because of the well-established relationship between $curl_z \tau$ and Ekman convergence and divergence, and the relationship between u_*^3 and the mechanical mixing of the sea by the overlying atmosphere. This same analysis was used in this study to identify storm tracks and to determine the extent to which synoptic storm activity mixes and/or pumps the ocean.

From the ten years of six-hourly surface wind data, a monthly climatology of both u_*^3 and $curl_z \tau$ was established.

Using this climatology, u_*^3 and $\text{curl}_z\tau$ anomalies were also calculated for each month of the ten year period. The remainder of this paper is devoted to describing the procedures used in data processing, data analyses, and interpreting the patterns of climatological u_*^3 and $\text{curl}_z\tau$. A case study, which compares the change in anomalous SST during the winter season 1976-1977 to the averaged anomalous u_*^3 and $\text{curl}_z\tau$ for that period, will also be discussed.

II. DATA SET DESCRIPTION AND ANALYSES

A. DATA ACQUISITION AND PROCESSING

The wind data were obtained from FNOC through Scripps Institution of Oceanography and were based on six-hourly surface pressure analyses over the North Pacific Ocean. The first seven years (1969-1975) of data were produced by a private company under a contract from FNOC (Mendenhall, Holl and Cuming, 1978), with the last three years (1976-1978) coming directly from FNOC operational analyses. The surface pressure analyses were derived by using previously computed surface pressure analyses as a first guess and upgrading the analyses with surface pressure and wind velocity observations from the U.S. National Climatic Center land and ship data. The winds were adjusted to an elevation of 19.5 meters above sea level. However, one weakness in using surface pressure analyses is that an underestimation of high wind speeds may result (Lazanoff and Stevenson, 1978). From these data, u (eastward) and v (northward) wind components were extracted from grid points on the FNOC 63x63 Northern Hemisphere polar stereographic array between 0^{o} and 70^{o}N and from 120^{o}W to 100^{o}E (North Pacific Ocean area). The grid spacing varies from 381 km at 60^{o}N to 208 km at the equator. At each grid point there were four daily observations (00GMT, 06GMT, 12GMT, 18GMT) throughout the ten-year period.

B. TREATMENT OF MISSING DATA

The maximum number of consecutively missing observations was seven and this happened twice in the ten-year period. Overall, less than six percent of the total observations was missing. Figure 1 shows the percent of missing data each month for the ten year-period. It should be quite apparent from the figure when the special analysis produced by the private company terminated (1975) and when the operational data from FNOC began (1976). All missing data groups were filled by interpolating linearly from preceding and succeeding map times.

C. DETRENDING AND FILTERING OF DATA

The next step was to detrend and filter the data. By detrending the data any linear trends were removed. After the appropriate slopes and intercepts were calculated, the equation used in detrending was

$$Y_m = y_m - (at_m + b) \qquad \text{(II-1)}$$

where Y_m is the detrended value at the m^{th} time observation, y_m is the original observation, a is the slope, b is the intercept and $t_m = (m-1)\Delta t$, with Δt = six hours, being the time interval. The method of least squares applied to each grid-point forms the basis of the detrending program used.

In order to extract synoptic storm activity from the ten-year period, a 41-point symmetric high-pass filter was

applied to the detrended time series of velocity components at each grid point. The filtering equation was

$$u_{i,j}(t_m) = w_o u_{i,j}(t_m) + \sum_{k=1}^{20} (u_{i,j}(t_{m+k}) + u_{i,j}(t_{m-k}))w_k$$

$$v_{i,j}(t_m) = w_o v_{i,j}(t_m) + \sum_{k=1}^{20} (v_{i,j}(t_{m+k}) + v_{i,j}(t_{m-k}))w_k \qquad \text{(II-2)}$$

where $u_{i,j}(t_m)$ and $v_{i,j}(t_m)$ represent the u and v wind components respectively at the grid point (i,j) at the time t_m, and w_k are the coefficients for the filter. The coefficients, shown in Table I, were computed using the following Gaussian filter,

$$w_o = 1-\Delta t(2\pi\sigma^2)^{-\frac{1}{2}}$$

$$w_k = -\Delta t(2\pi\sigma^2)^{-\frac{1}{2}} \exp(-t_k^2/2\sigma^2) , \qquad \text{(II-3)}$$

where $t_k = k\Delta t$, k=1,...20, σ = 1.5 days and Δt = .25 days. The response of the filter is shown in Figure 2. The filter is sensitive to periods of ten days or less or frequencies greater than 0.10 cycles day^{-1}. The significant response is for periods of less than five days. This is designed to extract events within the synoptic time scale.

TABLE I. Filter coefficients and corresponding weights.

k	w_k
0	0.933510
1	-0.065573
2	-0.062897
3	-0.058678
4	-0.053241
5	-0.046985
6	-0.040328
7	-0.033666
8	-0.027335
9	-0.021586
10	-0.016580
11	-0.012385
12	-0.008998
13	-0.006359
14	-0.004370
15	-0.002921
16	-0.001899
17	-0.001201
18	-0.000739
19	-0.000442
20	-0.000257

III. CALCULATIONS PERFORMED

A. EQUATIONS

Calculations of friction velocity cubed (u_*^3) and the curl of the wind stress ($curl_z\tau$) were made four times a day at every grid point using both the total and filtered wind components. The equations employed for the calculations were:

$$u_*^3 = [C_D(u^2 + v^2)]^{3/2} \qquad \text{(III-1)}$$

$$curl_z\tau = m^2\left[\frac{\partial}{\partial x}\left(\frac{\tau_y}{m}\right) - \frac{\partial}{\partial y}\left(\frac{\tau_x}{m}\right)\right] \qquad \text{(III-2)}$$

where,

$$\begin{aligned}
C_D &= (0.75 + 0.00067(u^2+v^2)^{\frac{1}{2}})10^{-3} \\
m &= (1+\sin\phi_t)/(1+\sin\phi) \\
\tau_x &= -\tau_\lambda \sin\lambda_* - \tau_\phi \cos\lambda_* \\
\tau_y &= \tau_\lambda \cos\lambda_* - \tau_\phi \sin\lambda_* \\
\tau_\lambda &= \rho_a C_D (u^2+v^2)^{\frac{1}{2}} u \\
\tau_\phi &= \rho_a C_D (u^2+v^2)^{\frac{1}{2}} v \\
\phi &= \pi/2 - 2\arctan[(x^2+y^2)^{\frac{1}{2}}/a(1+\sin\phi_t)] \\
\lambda_* &= \arctan(y/x) \ .
\end{aligned} \qquad \text{(III-3)}$$

In the above, a is the radius of the earth, ϕ_t is the true latitude of the polar stereographic projection, 60^o, and

the air density ρ_a was taken as a constant 1.3×10^{-3} gm cm^{-3}. Other expressions used included the non-dimensional drag coefficient C_D (Garratt, 1977), the zonal and meridional stress components τ_λ and τ_φ, and the map factor m, which represents the coordinate transformation from spherical coordinates (λ,φ) to polar stereographic coordinates (x,y) (see Haltiner, 1971, p.13). The same equations were used on both the filtered and total wind fields with the appropriate u and v components. In the finite difference approximations used to calculate $\text{curl}_z\tau$, centered differences on a staggered grid on the polar stereographic projection were used. If $\tau_{X_{i,j}}$ and $\tau_{Y_{i,j}}$ are defined on the array i=1,... IM and j=1,...JM, then $\text{curl}_z\tau$ is defined on a staggered grid by

$$\begin{aligned}(\text{curl}_z\tau)_{i,j} = (\tilde{m}_{i,j})^2 [&\tfrac{1}{2}((\tau_Y/m)_{i+1,j+1} + (\tau_Y/m)_{i+1,j}) \\ &- \tfrac{1}{2}((\tau_Y/m)_{i,j+1} + (\tau_Y/m)_{i,j}) \\ &- \tfrac{1}{2}((\tau_X/m)_{i,j+1} + (\tau_X/m)_{i+1,j+1}) \\ &+ \tfrac{1}{2}((\tau_X/m)_{i,j} + (\tau_X/m)_{i+1,j})]\end{aligned} \qquad \text{(III-4)}$$

where $\tilde{m}_{i,j}$ is an averaged map factor defined by

$$\tilde{m}_{i,j} = \frac{(m_{(i+1,j)} + m_{(i+1,j+1)} + m_{(i,j+1)} + m_{(i,j)})}{4} \qquad \text{(III-5)}$$

and where the range of i,j is i=1,...IM-1 and j=1,...JM-1.

B. u_*^3 AND $CURL_z\tau$ DEVELOPMENT

As will be shown later, a measure of the monthly mean storminess (which will be used to develop a ten year climatology) and the corresponding storm tracks can be calculated from the high-pass filtered wind components. Since u_* represents friction velocity, u_*^3 was used because it is a measure of the mechanical mixing in the ocean due to the overlying atmospheric circulation. Elsberry and Camp (1978) obtained a high correlation between u_*^3 and mixing of the ocean. A u_*^3 value was calculated for each data point and for each observation. For comparison purposes, u_*^3 calculations were performed using both the total and the filtered wind components.

Curl calculations were also performed on both the total and the filtered wind fields. The objective of calculating $curl_z\tau$ from the filtered wind data was to see if there was a contribution to Ekman pumping related solely to the monthly mean location of synoptic storm activity. It should be noted that the above calculations of u_*^3 and $curl_z\tau$ using the high-pass filtered wind components reveal the effects of the synoptic activity alone, i.e., in the absence of any low frequency or mean flow. None of the interaction terms (between high and low frequencies) which appear in the nonlinear quantities u_*^3 and $curl_z\tau$ are included. This point is discussed in the conclusion section below.

C. DESCRIPTION OF CLIMATOLOGY AND ANOMALIES

With u_*^3 and $curl_z\tau$ values calculated for each grid point and for each observation, a monthly mean for each month between January 1969 and December 1978 was calculated. This was done using both the filtered and total wind components. It should be noted that the monthly mean u_*^3 and $curl_z\tau$ values for January 1969 and December 1978 calculated from the filtered data consist of only 26 days. This was necessary due to the 41-point symmetric high-pass filter which needed 5 days (20 observations in time) on either side of the point to be filtered.

With the monthly means computed, the next step was to develop a climatology and then to use the climatology and monthly means in establishing anomalies. A climatology based on the ten years of data was developed for each month of the year by averaging all the u_*^3 and $curl_z\tau$ monthly means for January, then February, and continuing through December. With monthly means and climatology values, anomalies of u_*^3 and $curl_z\tau$ were created by subtracting the appropriate climatology from each monthly mean throughout the ten-year period. In the next section attention will be focused on climatological values of u_*^3 and $curl_z\tau$ as calculated from total and filtered wind components. After that, a relationship between anomalous storm activity and the development of anomalous SST's will be examined.

IV. DISCUSSION AND RESULTS

A. EXAMINATION OF u_*^3 and $CURL_z\tau$ CLIMATOLOGY

In this section, values of climatological u_*^3 calculated from the high-pass filtered wind components will be shown to be a good representation of storminess and storm tracks over the ten-year period. On the other hand, values of climatological $curl_z\tau$ are not as conclusive. The u_*^3 and $curl_z\tau$ parameters were used because of their role in mixing and pumping of the ocean, respectively. The 12 months of climatological u_*^3 patterns calculated from the total wind field will be examined first, followed next by an examination of the climatological u_*^3 patterns calculated from the filtered wind field. The same procedure will be followed using $curl_z\tau$ results.

1. Relationship Between u_*^3 and u_*^3 from Filtered Data

Figures 3-14 are plots of climatological u_*^3 calculated from the total wind field. For January (Fig. 3) the maximum values of u_*^3 over water are centered at approximately 55^oN and 155^oE and 45^oN and 150^oW. In February (Fig. 4) there is little change with the two maxima remaining in nearly the same area and with the same magnitudes. By March (Fig. 5) the u_*^3 maxima begin to decrease in magnitude. This trend continues throughout the spring and into the summer (Figs. 6-11). Tropical disturbances begin appearing

in May (Fig. 7) and are present until October (Fig. 12). During October and November (Figs. 12, 13), the values of u_*^3 begin to increase with areas of maximum u_*^3 located particularly in the northwest Pacific and a secondary maximum located in the Gulf of Alaska. The maximum values of u_*^3 occur from late fall through early spring with little movement north or south. The u_*^3 values resulting from the trade winds south of 30°N are too small to appear in the figures because of the contour levels selected. The values of u_*^3 over the land masses (Siberia and Alaska) are of little interest in this study which is focused on synoptic storm activity.

Figures 15-26 are plots of climatological u_*^3 calculated from the filtered wind components. Notice that the contour levels are generally an order of magnitude smaller than in the corresponding Figs. 3-14. The filtered wind components represent storminess and monthly mean values of u_*^3 from filtered data are a measure of the monthly mean mixing of the ocean by synoptic storms. In January (Fig. 15) a well defined symmetric and coherent u_*^3 maximum lies at 45°N and 168°E. If maximum winds associated with a given storm occur near the center of the storm, then the axis of maximum u_*^3 represents the mean position of the storms (storm tracks) for that month. In this case, an associated storm track runs east-northeast from this center as indicated by the dashed lines. The months of February through April

(Figs. 16-18) also show well defined and coherent patterns of u_*^3. The storm tracks continue to stand out. Also, the maximum u_*^3 values remain nearly constant during this period. It is not until May (Fig. 19) that the magnitude lessens appreciably. This trend of decreasing magnitude continues through the summer until September (Fig. 23) is reached. After September the magnitudes begin increasing once again. This can be expected as synoptic storms become more developed and strengthen during early fall. In the months of May through November (Figs. 19-25) tropical storm activity is very prevalent. In addition to the decreasing magnitude of u_*^3 during the summer, there is a slight northward and eastward movement as synoptic storm activity weakens and moves north. The plots clearly show that the main center of storminess, throughout the year, lies in the northwest Pacific Ocean region.

Now the question may be raised as to what part of the total u_*^3 field is due to the synoptic scale part of the frequency spectrum as determined by u_*^3 calculated from the high-pass filtered wind data. Table II shows, for each month, the percent of the total monthly mean u_*^3, that is due to synoptic storm activity. These values were obtained by dividing the u_*^3 value computed from the filtered wind components by the appropriate u_*^3 value computed from the total wind components. For instance, the January value was calculated by dividing the maximum oceanic value in Fig. 15

TABLE II. Monthly importance of filtered u_*^3 relative to the total u_*^3 field in percent.

Month	Percent Importance
Jan	33
Feb	34
Mar	34
Apr	37
May	20
Jun	20
Jul	20
Aug	30
Sep	40
Oct	30
Nov	32
Dec	50

(13×10^4 $(cm/s)^3$) by the corresponding maximum in Fig. 3 (4×10^5 $(cm/s)^3$) resulting in 0.33 or 33 percent. It was found that the overall average was 32 percent. During the stormier months of September through April the average was 36 percent with a single monthly high of 50 percent in December. Elsberry and Camp (1978) found significantly greater u_*^3 values related to synoptic storms. The discrepancy is most likely due to the omission of interactions between high and low frequencies in the u_*^3 values calculated from filtered data in this study. That is, the calculations from the high pass filtered data used in this study show the effects of storms in the absence of a mean (or low frequency) flow, whereas the Elsberry and Camp study shows the effects of the storms in the presence of a mean flow.

The major result of the above calculations is twofold and can be summarized as follows. First, the

climatological values of monthly mean u_*^3 calculated from the high pass filtered wind components clearly reveal large, spatially coherent areas of synoptic storm activity. Second, the magnitude of the u_*^3 which comes from the synoptic part of the spectrum alone is a sizable fraction, approximately one-third, of the total u_*^3.

2. Relationship Between $Curl_z\tau$ and $Curl_z\tau$ from Filtered Data

Figures 27-38 are the monthly climatological maps of $curl_z\tau$ calculated from the total wind field. Areas of positive curl are shaded. A strong west to east band of positive $curl_z\tau$ exists in all months between 40°-60°N. These bands are especially strong during the winter months of December (Fig. 38) through March (Figs. 27-29) with a north to south narrowing of the band during the summer months of May through September (Figs. 31-35). The areas of maximum positive $curl_z\tau$ are widespread but appear to be centered in two main areas. One is centered at 55°N and 160°E with the other centered at 55°N and 140°W. These areas become less organized in the spring and summer months of March through October (Figs. 29-36). This broad region of positive wind stress curl coincides with the location of the semi-permanent Aleutian Low and the known location of mid-latitude cyclonic activity.

The main area of negative $curl_z\tau$ lies immediately south of the positive $curl_z\tau$ area in the general location of the semi-permanent subtropical high between 20°-40°N. This

west to east band has no seasonal preference in either area or magnitude.

The monthly maps of $\text{curl}_z\tau$ calculated from the high-pass filtered data and averaged over the ten years are shown in Figs. 39-50. A broad area of positive $\text{curl}_z\tau$ is found in mid-latitudes similar to the regions of filtered u_*^3 shown previously. However, the patterns are much more "noisy" and somewhat less coherent than the u_*^3 patterns. During the months of January and February (Figs. 39, 40) the maximum positive $\text{curl}_z\tau$ areas occur at 40°N between 150°-180°E. As spring, represented by March through June, (Figs. 41-44) approaches, the maximum positive $\text{curl}_z\tau$ shifts to the north with the general migration of the mean storm tracks. The $\text{curl}_z\tau$ reaches its maximum positive value in March (Fig. 41). Beginning in April and continuing through November (Figs. 42-49) the center of maximum $\text{curl}_z\tau$ remains quasi-stationary between 40°-45°N and 150°-170°E before shifting south and intensifying in December (Fig. 50). Also, note that during the typhoon and tropical storm season of June through October (Figs. 44-48), large positive and negative areas of $\text{curl}_z\tau$ exist in the tropical areas especially off Baja, California (10°-20°N, 100°-140°W) and in the Philippine and North China Sea areas (10°-30°N, 120°-160°E).

The broad band of negative $\text{curl}_z\tau$ to the north of the main storm track behaves in the same manner as the positive $\text{curl}_z\tau$. During the months of December (Fig. 50) and

January through February (Figs. 39, 40), the center of the region of negative $curl_z\tau$ lies between 45°-55°N and between 150°E-150°W. In the summer months (Figs. 43-48) it moves north, while in July and August (Figs. 45, 46) the negative $curl_z\tau$ is disorganized and very weak. Finally the negative $curl_z\tau$ becomes more organized during the fall (Figs. 47-49).

As with u_*^3 it is important to calculate the percent of the total $curl_z\tau$ field due to storminess, or those $curl_z\tau$ values calculated from filtered wind components. Table III gives a monthly percent obtained by dividing the values of $curl_z\tau$ calculated from the filtered data by the values of $curl_z\tau$ calculated from the total wind field. The procedure used in obtaining Table III was the same as used for Table II.

TABLE III. Monthly importance of filtered $Curl_z\tau$ relative to the total $Curl_z\tau$ field in percent.

Month	Percent Importance
Jan	2
Feb	3
Mar	16
Apr	13
May	10
Jun	15
Jul	10
Aug	10
Sep	10
Oct	10
Nov	5
Dec	3

The mean value for the entire year is 8.5 percent which is significantly lower than that obtained for u_*^3.

Further comparisons between u_*^3 and $curl_z \tau$ calculated from the high-pass filtered data show a major difference in spatial patterns. The u_*^3 field is somewhat more coherent and far less "noisy". Synoptic storm areas and associated tracks are more easily discernible and the patterns are very smooth. Since storminess contributes relatively more to the total u_*^3 field, this result correlates well. The major result of the foregoing examination shows that the contribution of synoptic storm activity to vertical turbulent mixing (u_*^3) of the ocean is significant, while the contribution of synoptic activity to Ekman pumping ($curl_z \tau$) of the ocean is much less significant. In the next section an example of SST anomalies will be compared to filtered u_*^3 and filtered $curl_z \tau$ anomalies.

B. CASE STUDY OF ANOMALOUS STORMINESS AND ANOMALOUS SST

It is reasonable to expect that at the same location where there is a maximum of wind mixing, the SST decreases will be largest. This hypothesis is based on a correlation of upward heat flux with wind speed and that entrainment mixing contributes to SST decreases. White and Haney (1977) showed that during the autumn and winter of 1976-77 the storm forcing and SST evolution were both abnormal. Between 30°-50°N in the central portion of the ocean, the SST was 2 degrees colder than normal during the period in which the frequency of storms was 4-6 times greater than normal. To illustrate the relationship between the development of SST anomalies and anomalous storm activity, the SST anomalies that developed

during the winter season of 1976-77 will be compared to u_*^3 and $\text{curl}_z \tau$ anomalies calculated from the filtered wind components.

1. Relationship to be Tested

If the climatological u_*^3 or $\text{curl}_z \tau$ represents the normal or average synoptic storm activity over the ten-year period, then departures of these quantities from climatology may be related to SST anomalies through anomalous mixing and/or pumping of the ocean. The six-month period from mid-September 1976 through mid-March 1977 was examined to test the following equation:

$$\frac{\partial}{\partial t} (SST) = X \ , \qquad \text{(IV-1)}$$

where SST is the monthly mean sea-surface temperature anomaly (data kindly provided by Dr. J. Namias) and X represents the monthly mean u_*^3 or $\text{curl}_z \tau$ anomaly calculated from the filtered data. Integrating (IV-1) from the mid-September 1976 (SEP76) to mid-March 1977 (MAR77), the equation to test becomes

$$(SST)_{MAR77} - (SST)_{SEP76} = \overline{X} \qquad \text{(IV-2)}$$

where $\overline{X}$ is the integral of X over the six-month period. This integral was calculated from

$$\overline{X} = \frac{1}{6} \left[\frac{1}{2} (X_{SEP76} + X_{MAR77}) + \sum_{OCT76}^{FEB77} X \right]. \qquad \text{(IV-3)}$$

Using (IV-2), the time lag between atmospheric forcing and ocean response is taken into consideration.

2. Results of SST, u_*^3 and $\text{Curl}_z\tau$ Anomalies

Figure 51 (note difference in latitudinal coverage) is a plot of the SST anomaly change during the six-month period (left side of (IV-2)). Negative values are shaded indicating the development of colder than normal SST's, while positive values are unshaded. The main area of cold anomaly development lies between 25°-40°N and between 170°E-150°W. A secondary area extends southwestward off the west coast of California and Baja. Another area of consequence is centered at 32°N and 142°E. Two large areas of warm anomaly development are present. The first lies between 25°-40°N and between 150°-170°E. The second area lies off the west coast of North America and extends westward along the Aleutians into the Northwest Pacific.

Figure 52 shows the u_*^3 anomaly calculated from the filtered data and integrated over the six-month period (right side of (IV-2) with $\overline{X} = u_*^3$). Positive values are shaded, indicating greater than normal storminess during the period while negative areas are unshaded. The broad band of positive u_*^3 anomaly values lies between 20°-40°N and 150°E-150°W with an extension of positive values northward into the Gulf of Alaska. This pattern of storminess matches well with that described by Namias (1978) for the same period. Secondary maxima lie off the west coast of Mexico, in the tropics, and in the extreme western Pacific (130°E). Figure 53 shows $\text{curl}_z\tau$ anomalies calculated from the filtered data

and integrated over the six-month period (right side of (IV-2) with $X = \text{curl}_z \tau$). The shaded areas indicate positive anomalies of $\text{curl}_z \tau$ due to storminess. It is quite apparent that the pattern is much less coherent than the u_*^3 anomaly in Fig. 52 and the general spatial scale is quite different from the SST anomaly change in Fig. 51.

In comparing Figs. 52 and 53 to Fig. 51, the best correlation can be made between SST and u_*^3, although there is also some relation with $\text{curl}_z \tau$. The large area of SST anomaly decrease in the mid-latitudes compares favorably to the greater than normal amount of storminess in that area as measured by the filtered u_*^3 anomaly. Also, the large warm SST anomaly development in the Northwest Pacific coincides with the lack of storminess in that area as indicated by the negative u_*^3 anomaly. A weak correlation also exists between u_*^3 and the cold SST anomaly development off the California and Mexican coasts, with a better match in the West Pacific (130°E). The area of obvious conflict lies in the Gulf of Alaska where large positive u_*^3 values occur in the same place where positive SST anomalies developed. There is a good correlation with a negative anomalous wind stress curl in this area but the results are far from conclusive. Possible explanations for this warm SST development may be the low frequency part of the wind spectrum, anomalous surface heat fluxes or the northward advection of warm surface water.

The purpose of this case study was to see if a qualitative relation exists between SST anomaly changes

and anomalous storm activity. A study is now in progress to determine the statistical relationship between monthly SST anomalies and synoptic storm activity over the entire ten-year period.

V. CONCLUSIONS

The first conclusion drawn from climatological values of u_*^3 and $curl_z \tau$ computations is that the monthly mean u_*^3 calculated from filtered wind components is a good indicator of monthly storminess and storm tracks. Coherent patterns of u_*^3 and tracks of associated synoptic storms are easily discernible. In addition, the u_*^3 computed from filtered data constitutes a significant part (32%) of u_*^3 calculated from the total wind components. Therefore, a major conclusion is that the synoptic storm part of the frequency spectrum makes a large contribution to the atmospheric forcing of the upper ocean. On the other hand, maps of climatological $curl_z \tau$ calculated from the filtered wind components are much less significant (8.5%), more "noisy", less coherent, and are not as easy to associate with storm tracks. The atmospheric wind stress curl associated with the more permanent events having a time scale greater than that associated with synoptic storms appears to be more important.

A second more qualitative conclusion of this study indicates a relationship between anomalous u_*^3 from filtered data and SST anomalies. In the particular six-month period of study, areas of greater than normal synoptic storm activity were related to the development of negative or colder SST anomalies. Conversely, areas of lower than normal synoptic storm activity were related to warmer than normal SST anomaly

development. When comparing $curl_z$ calculated from the filtered data to the SST anomaly development, a much weaker relationship, if any, was apparent. It is hoped that the statistical study in progress will determine, more quantitatively, whether a relationship exists between monthly mean anomalies of SST and u_*^3 calculated from the filtered data.

As noted earlier, the fields of $curl_z$ calculated from both filtered and unfiltered data have a considerable amount of spatial noise. The noise comes from random data errors in time and space. One solution to this problem would be to have more accurate data, thereby reducing the error factor. Another solution would be to increase the data resolution. An increased resolution without increasing the accuracy in wind observations, however, would only make the noise problem associated with curl calculations worse or at best unchanged. Space smoothing could also be used. But according to Saunders (1975), coarse data resolution (i.e., space smoothed) may underestimate maxima and minima in the $curl_z$ by as much as 50 percent. The ideal situation would be to increase both the accuracy of the data and the space resolution.

As mentioned earlier, u_*^3 calculations from u and v components included the high pass effects only. This was an essential step in discussing storms and the climatology of storms. Interaction terms between low and high pass u and v components were not studied. The next step is to include the interaction terms of low and high pass filtered u and v components and then to determine their effects.

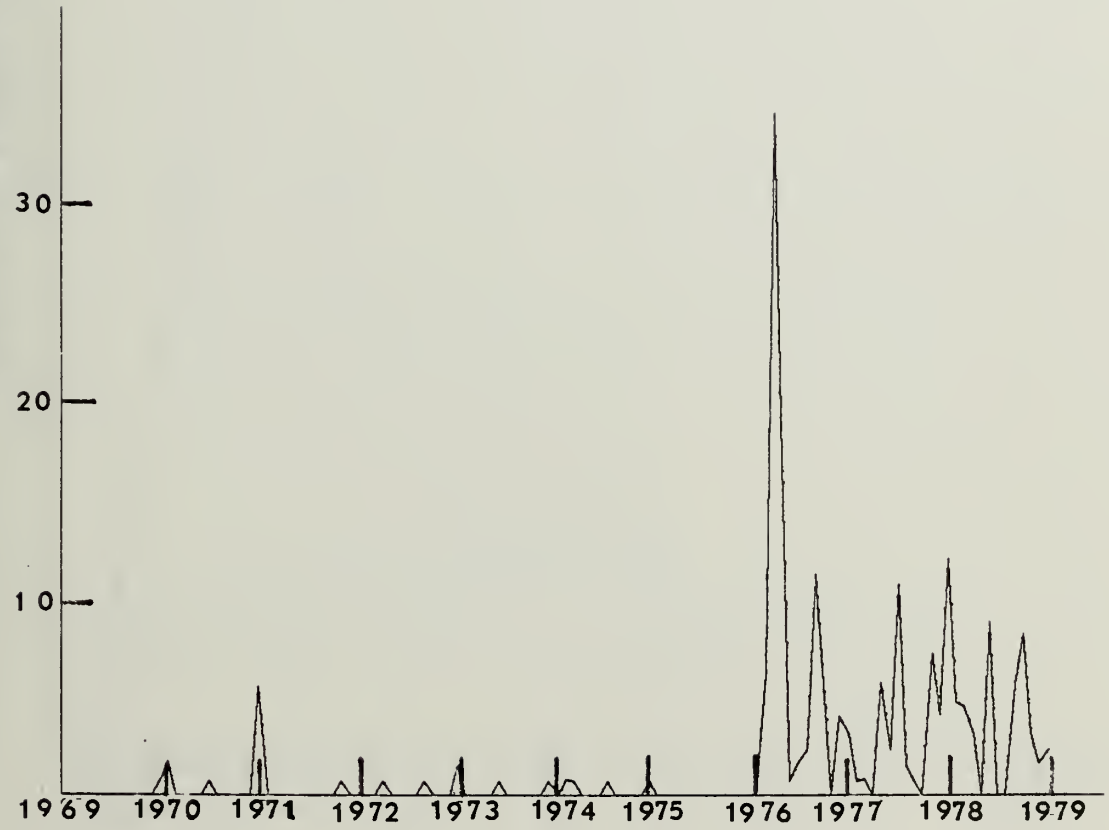

Figure 1. Percent of missing data by months for the period 1969-1978.

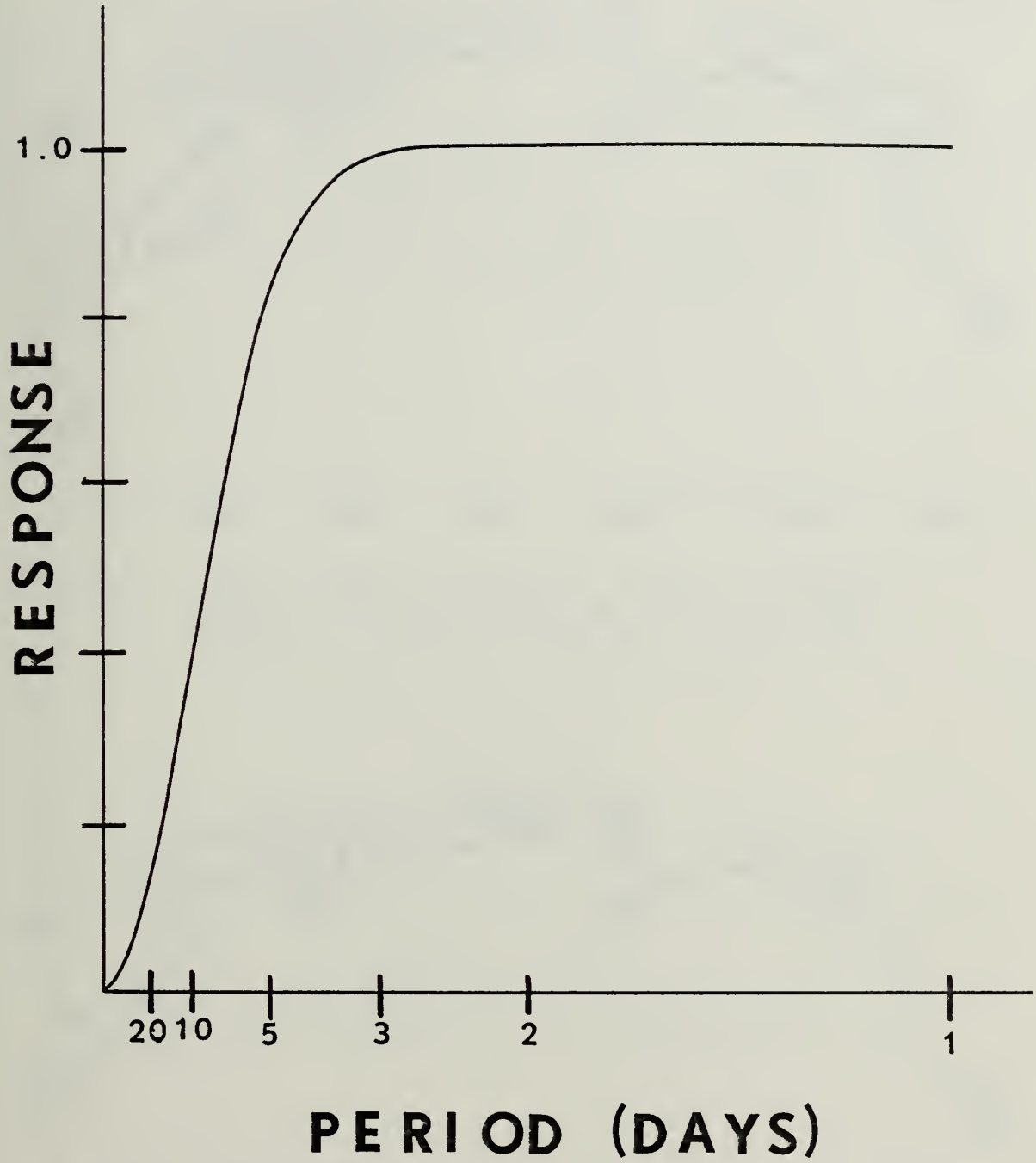

Figure 2. Response of the 41-point symmetric high-pass filter as a function of frequency.

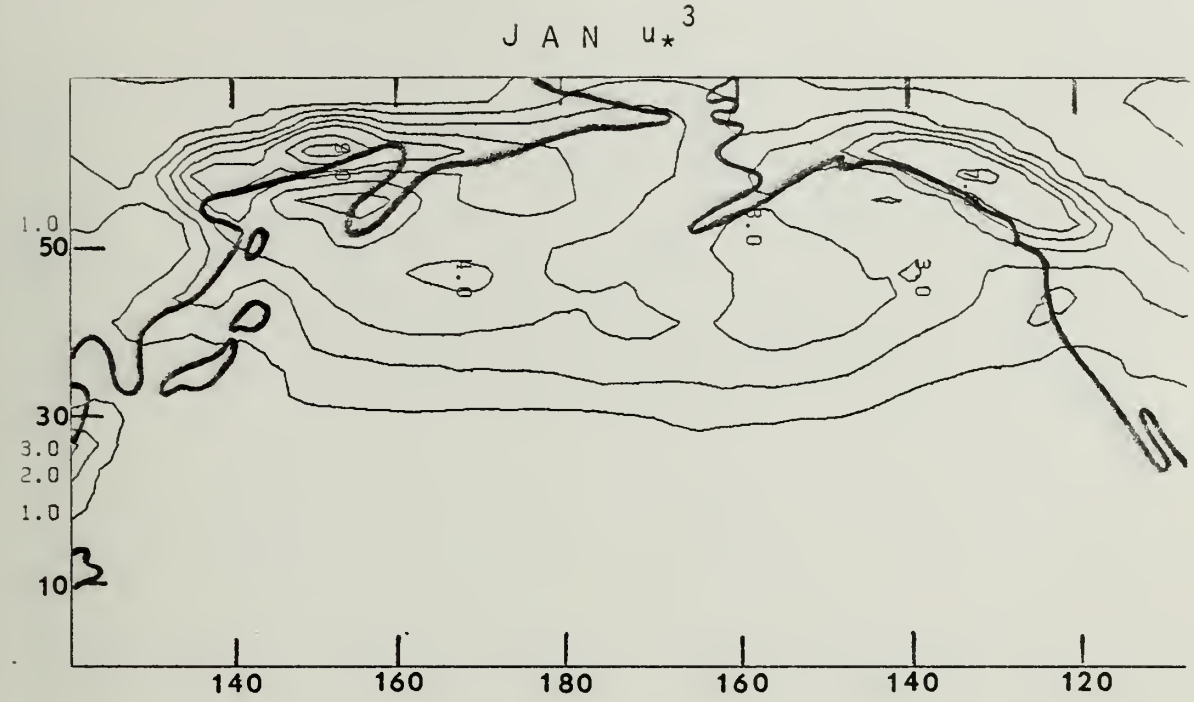

Figure 3. Climatological values of friction velocity cubed (u_*^3) from total u and v wind components. Contour values are 1.0,2.0,3.0, 4.0,5.0,7.0,9.0....x 10^5 $(cm/sec)^3$.

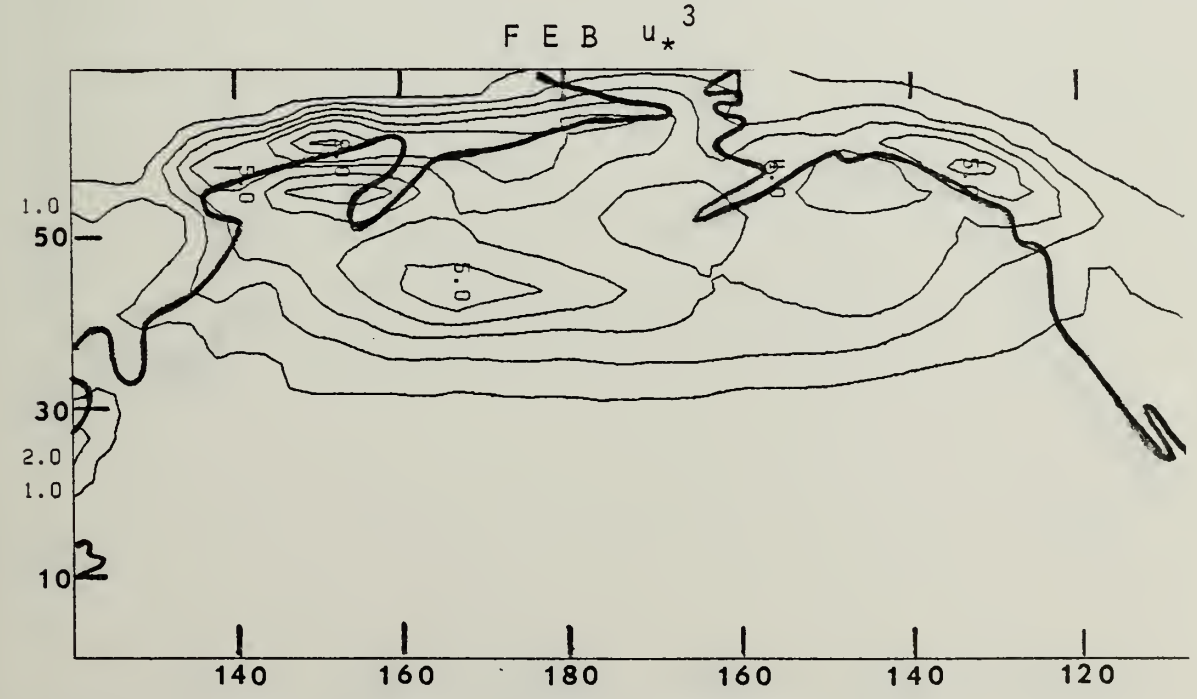

Figure 4. Same as Fig. 3 except for February.

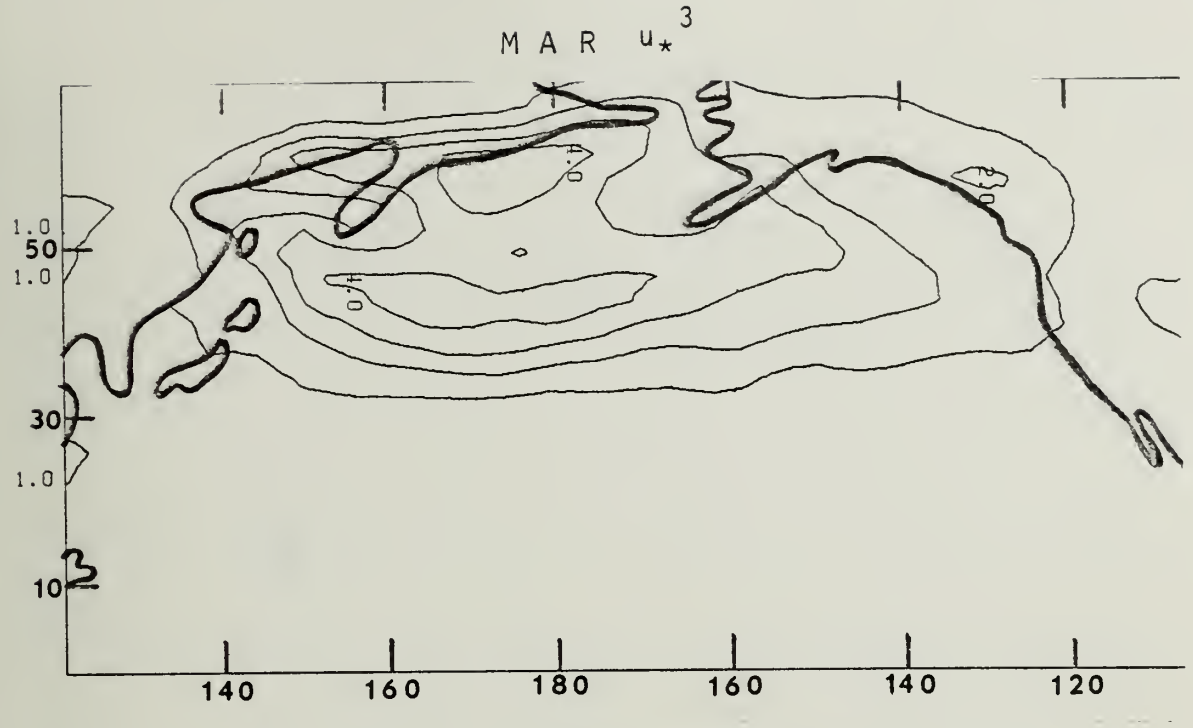

Figure 5. Same as Fig. 3 except for March.

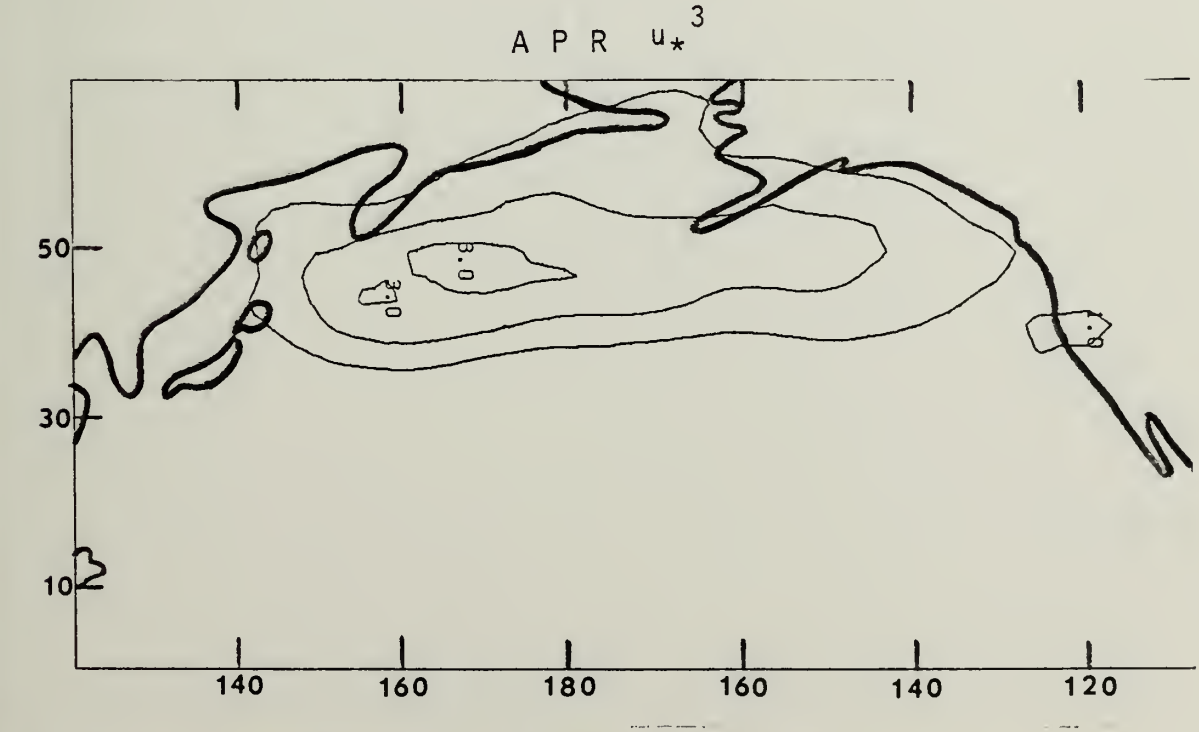

Figure 6. Same as Fig. 3 except for April.

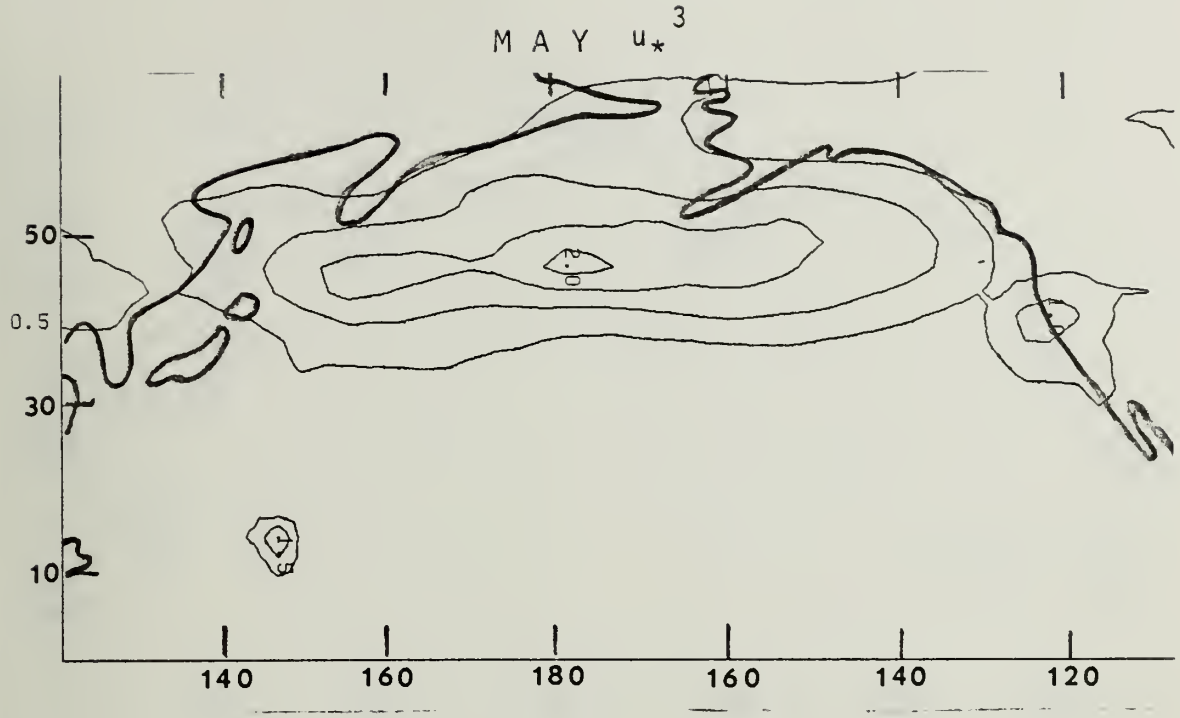

Figure 7. Same as Fig. 3 except contour values are $0.5,1.0,1.5,2.0,3.0,4.0....x\ 10^5$ $(cm/sec)^3$ and the month is May.

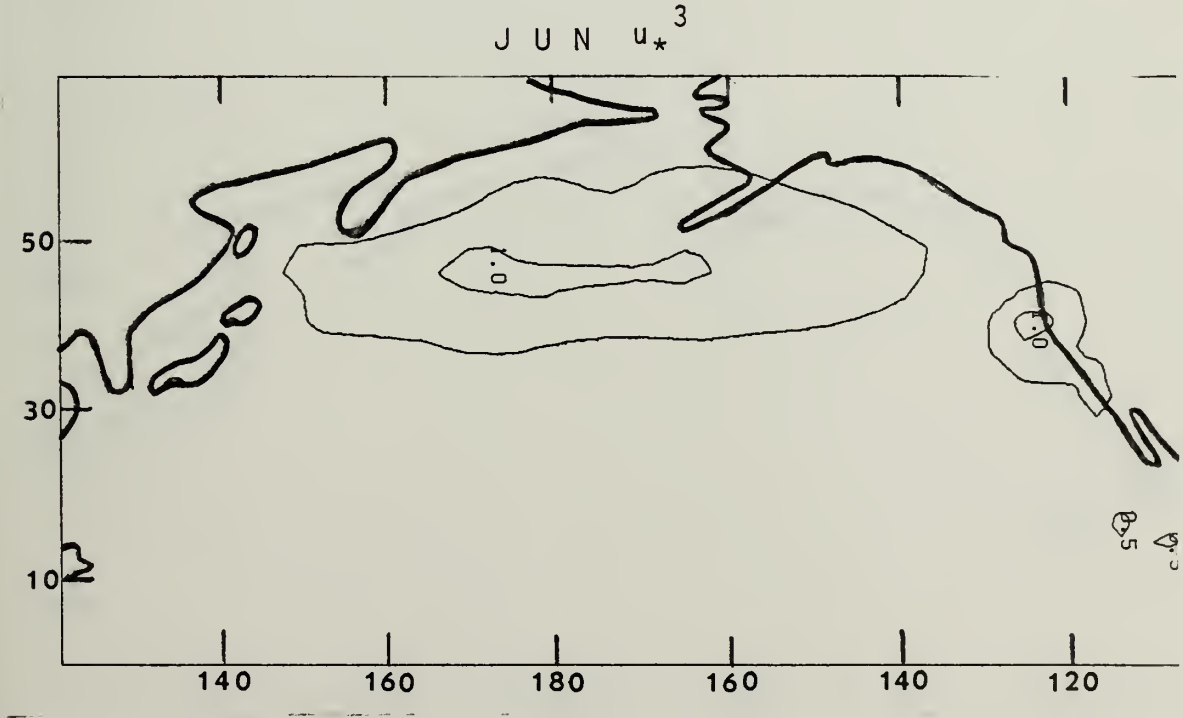

Figure 8. Same as Fig. 7 except for June.

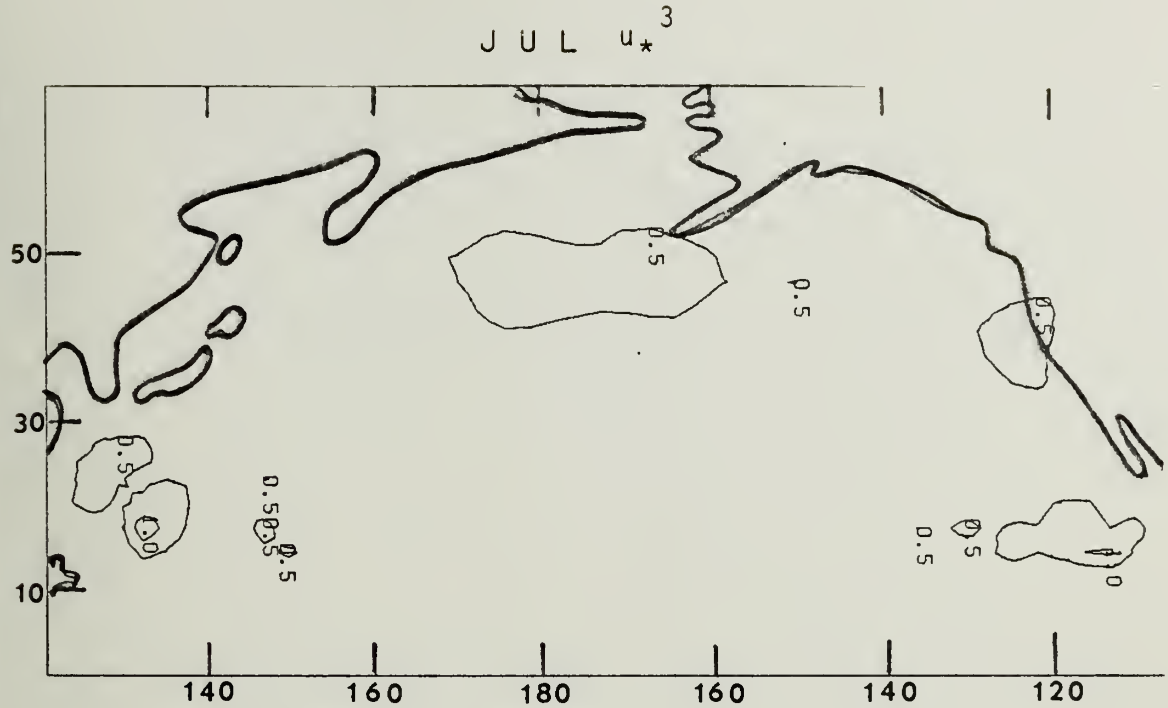

Figure 9. Same as Fig. 7 except for July.

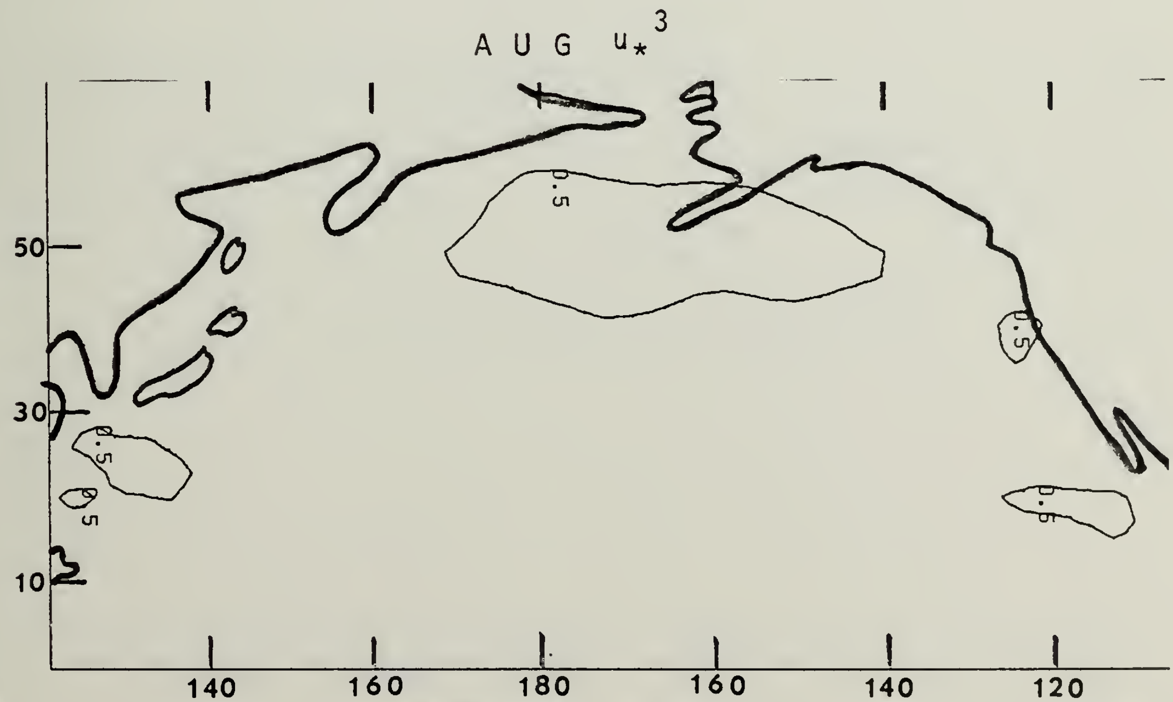

Figure 10. Same as Fig. 7 except for August.

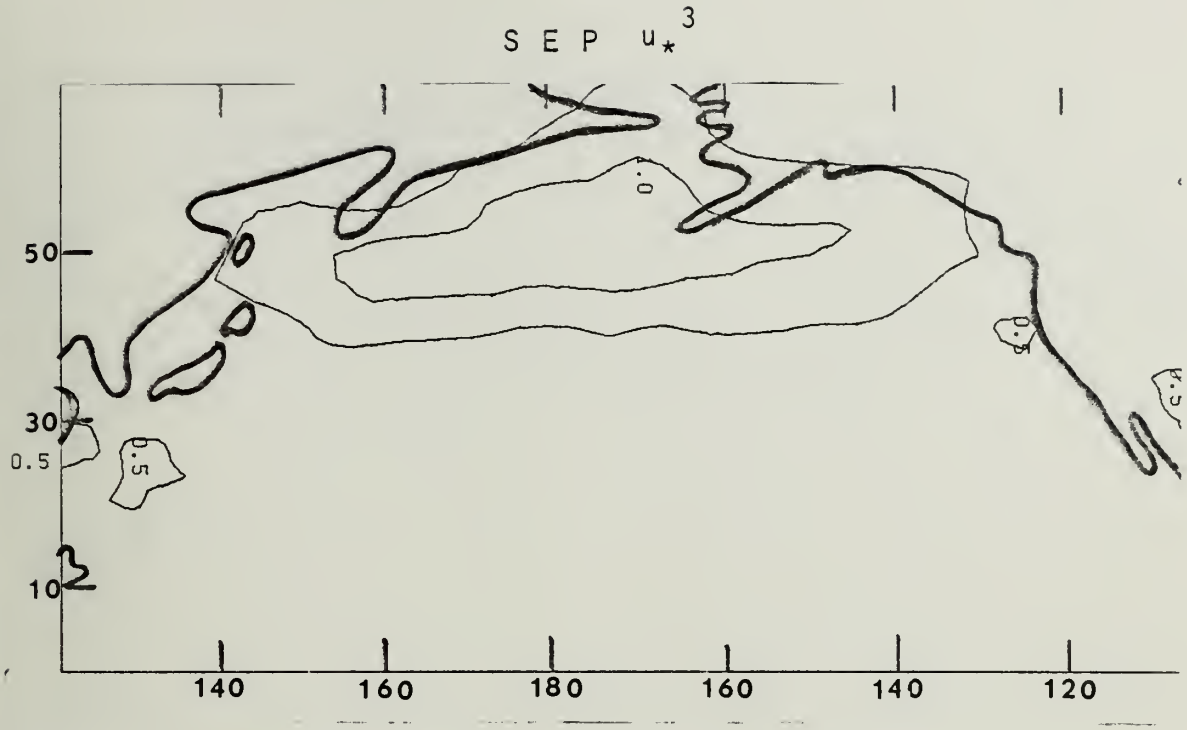

Figure 11. Same as Fig. 7 except for September.

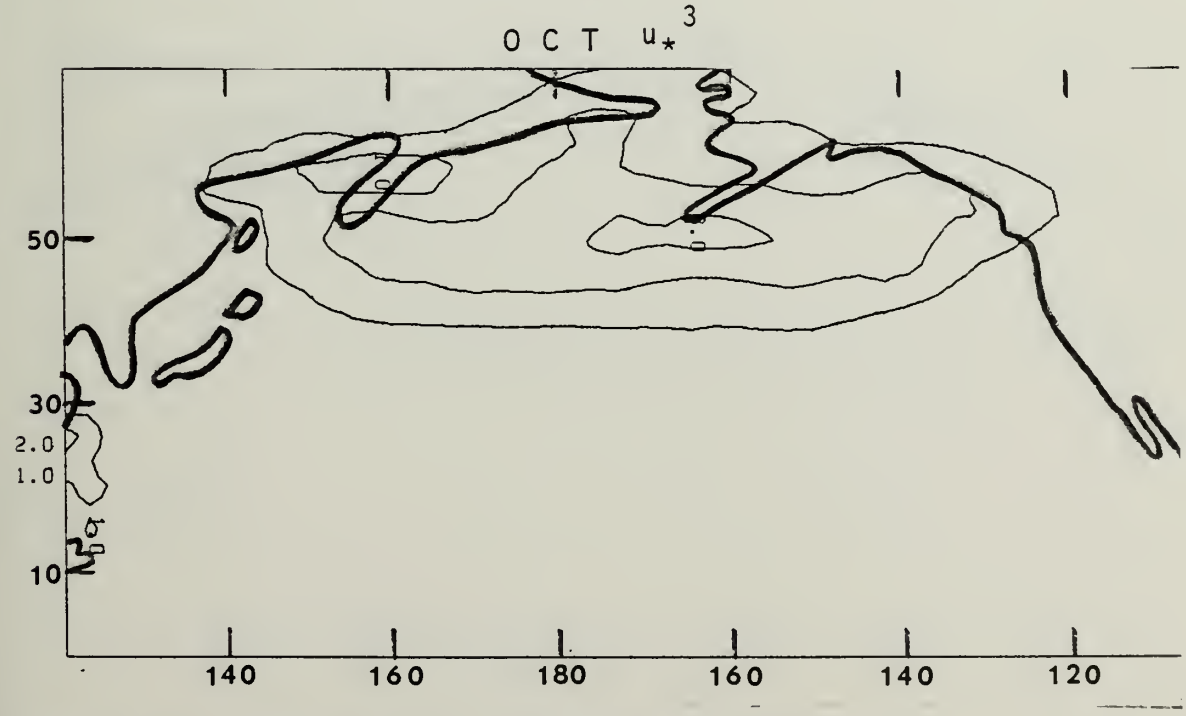

Figure 12. Same as Fig. 3 except for October.

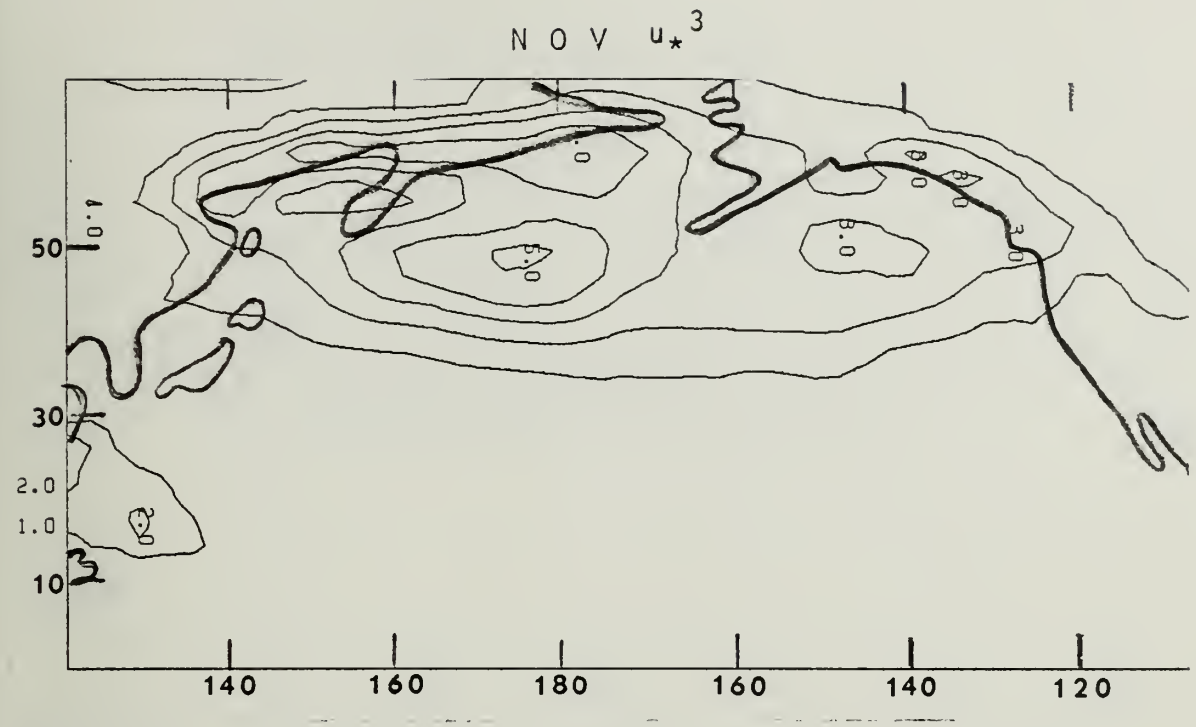

Figure 13. Same as Fig. 3 except for November.

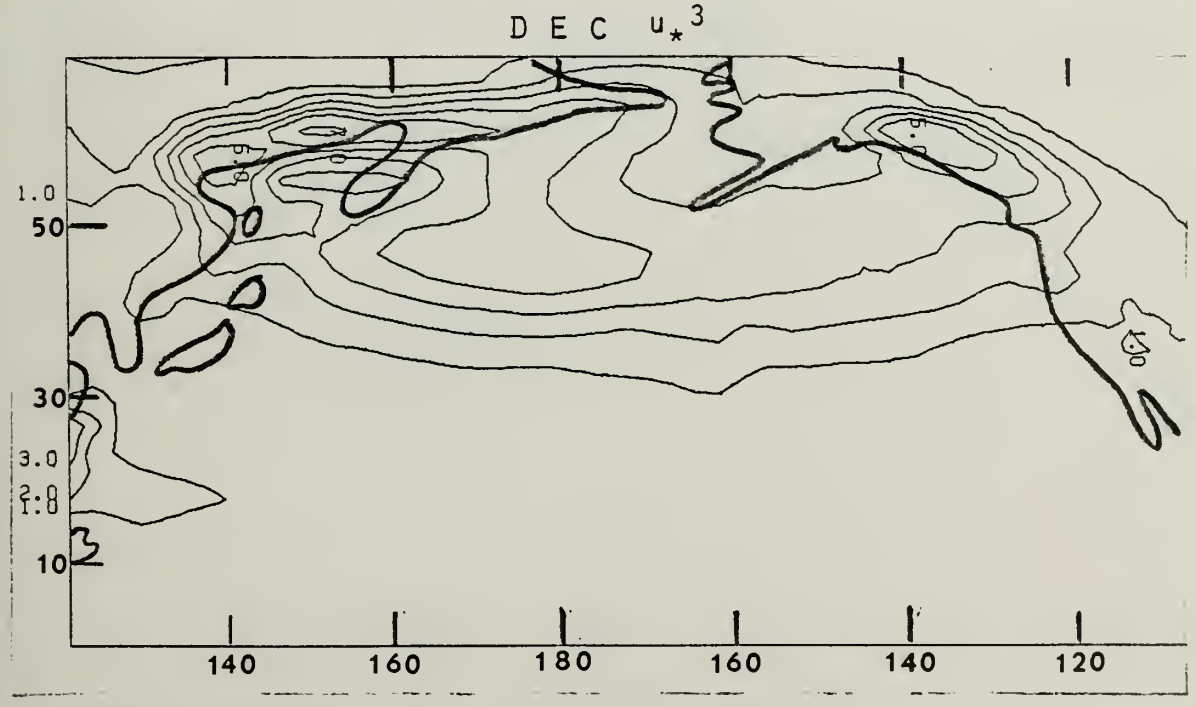

Figure 14. Same as Fig. 3 except for December.

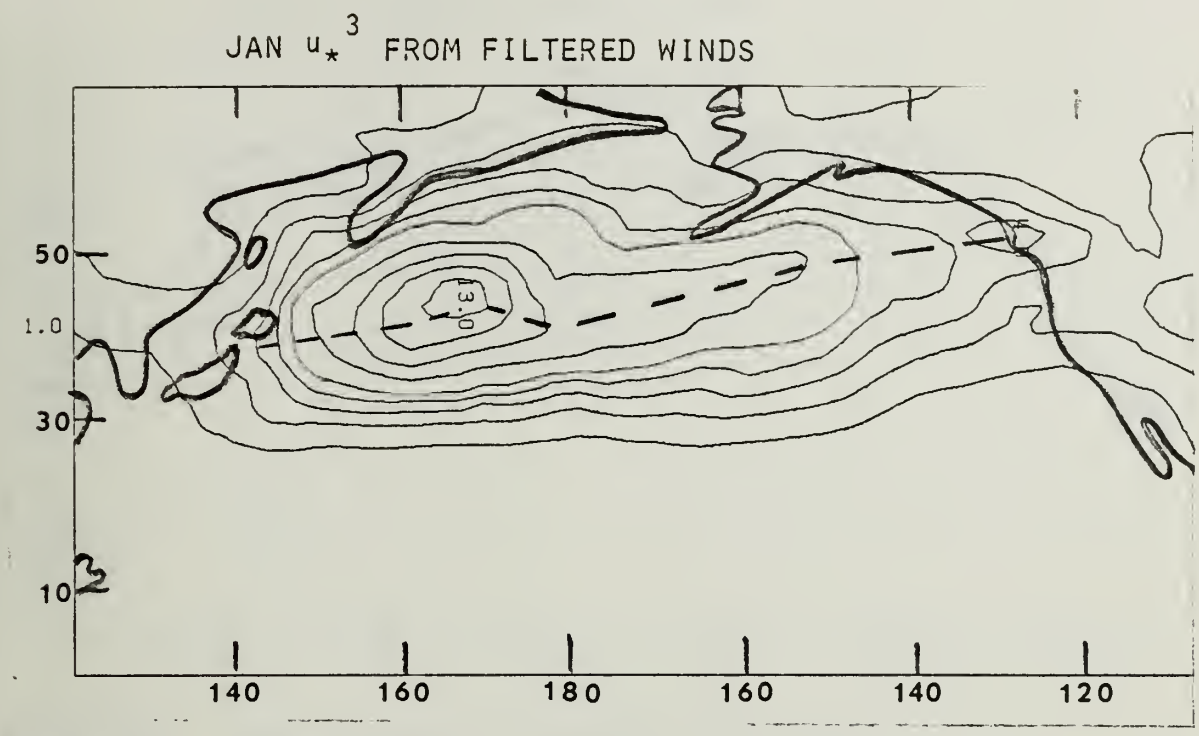

Figure 15. Climatological values of friction velocity cubed (u_*^3) from high-pass filtered u and v wind components. Dashed lines indicate storm tracks. Contour values are 1.0,2.0, 3.0,4.0,5.0,7.0,9.0....x 10^4 $(cm/sec)^3$.

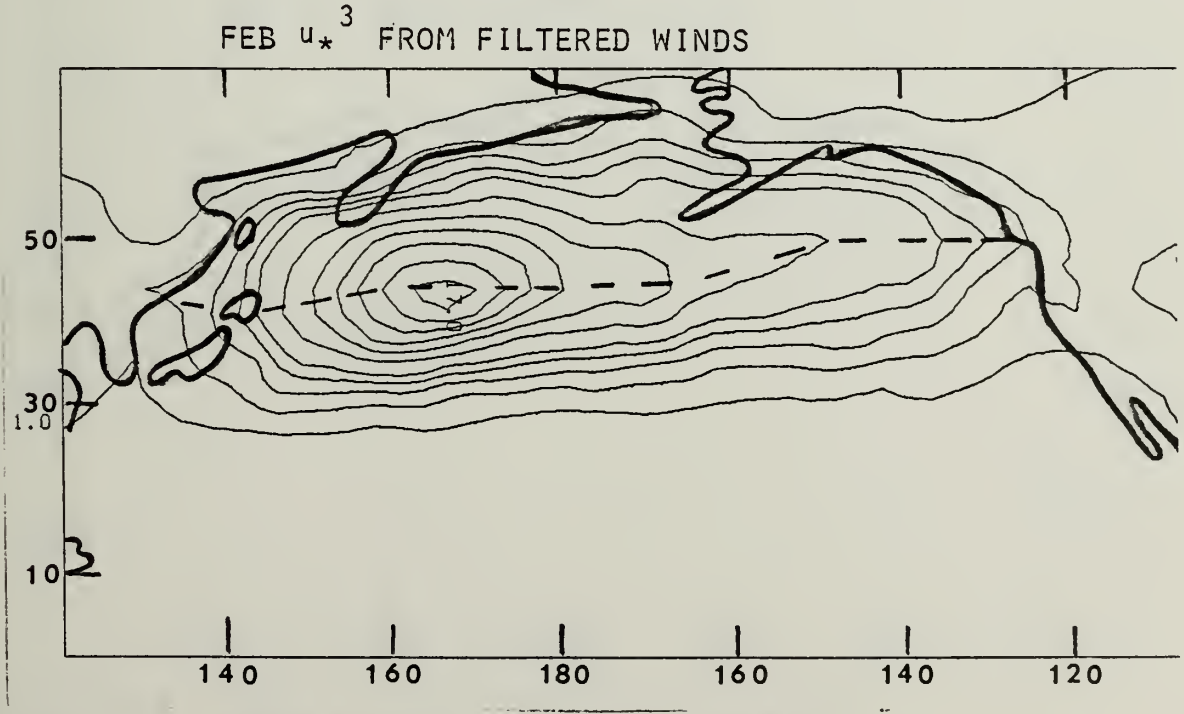

Figure 16. Same as Fig. 15 except for February.

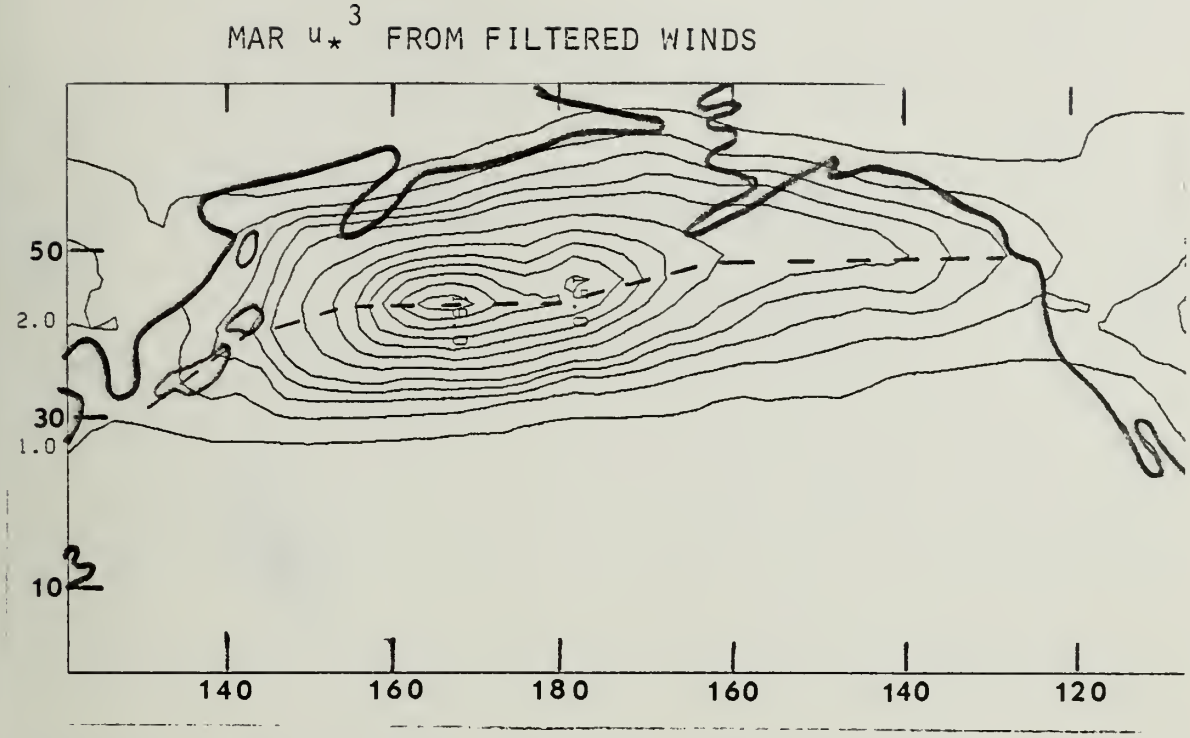

Figure 17. Same as Fig. 15 except for March.

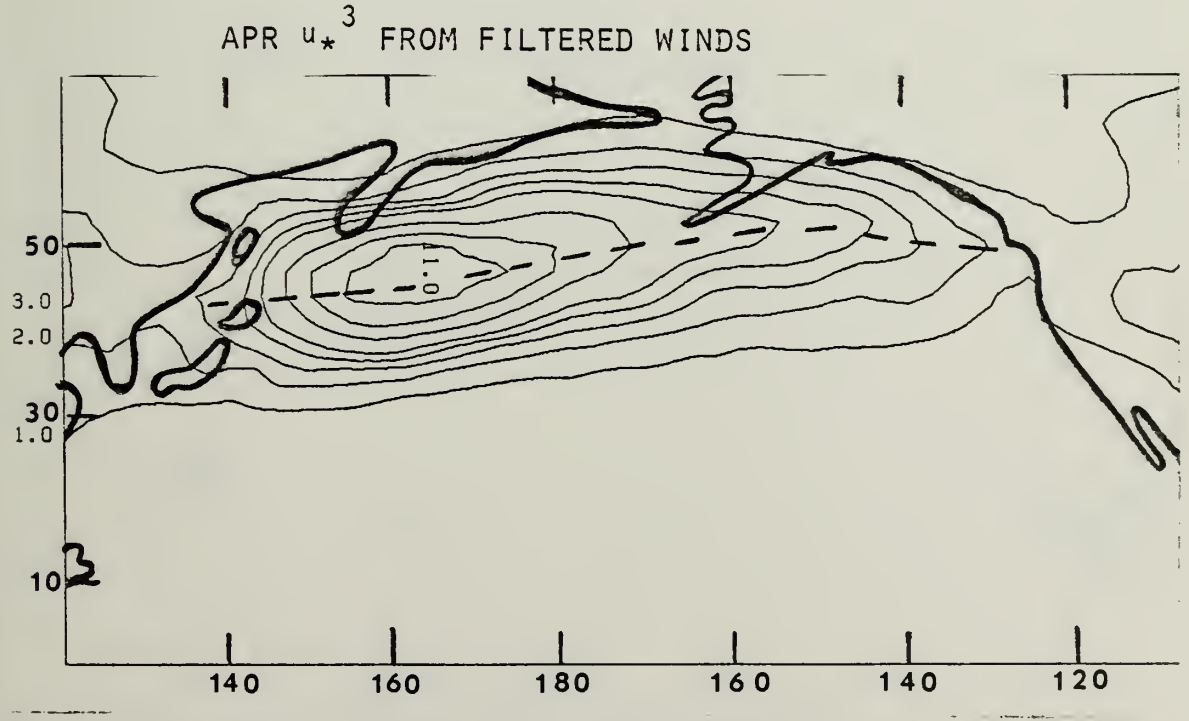

Figure 18. Same as Fig. 15 except for April.

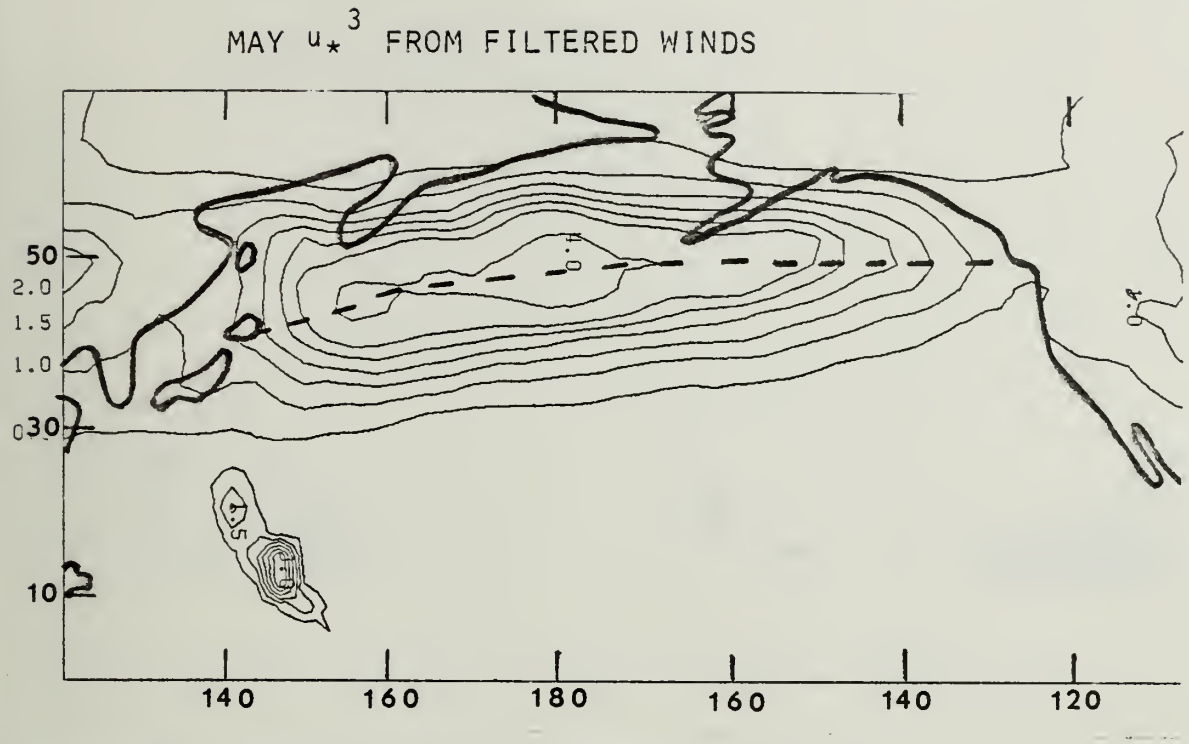

Figure 19. Same as Fig. 15 except contour values are 0.5,1.0,1.5,2.0,2.5,3.0,4.0,5.0....x 10^4 $(cm/sec)^3$ and the month is May.

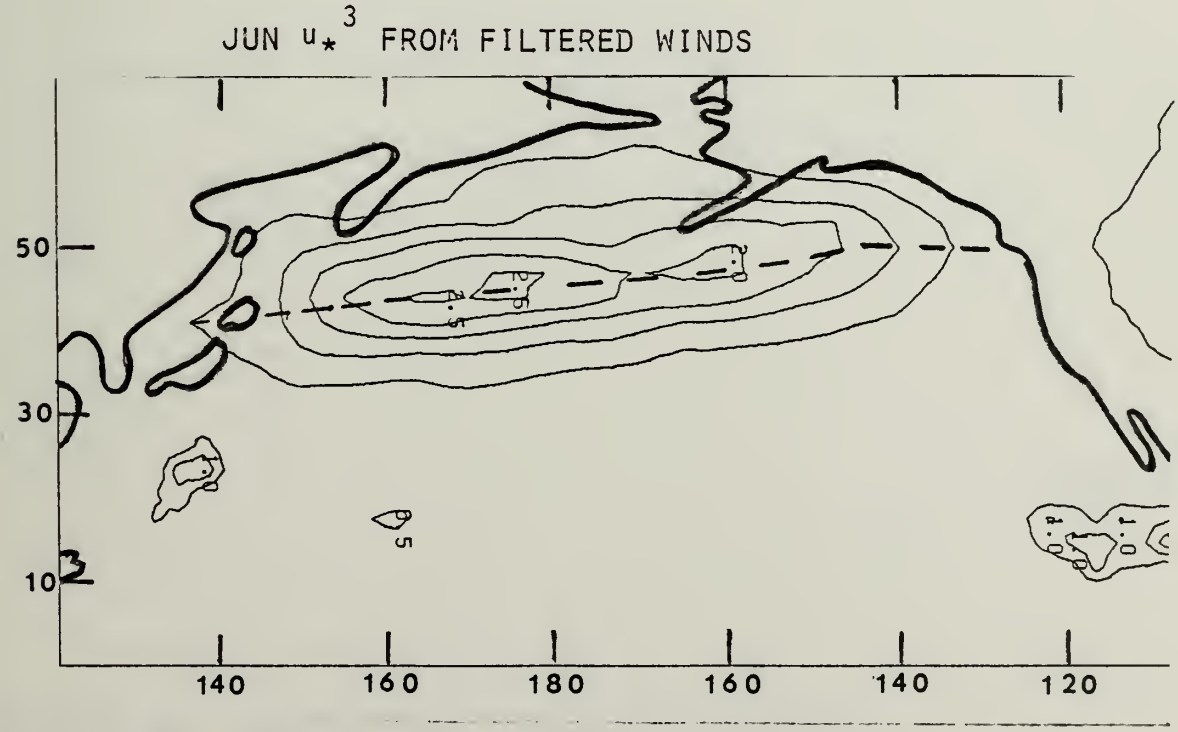

Figure 20. Same as Fig. 19 except for June.

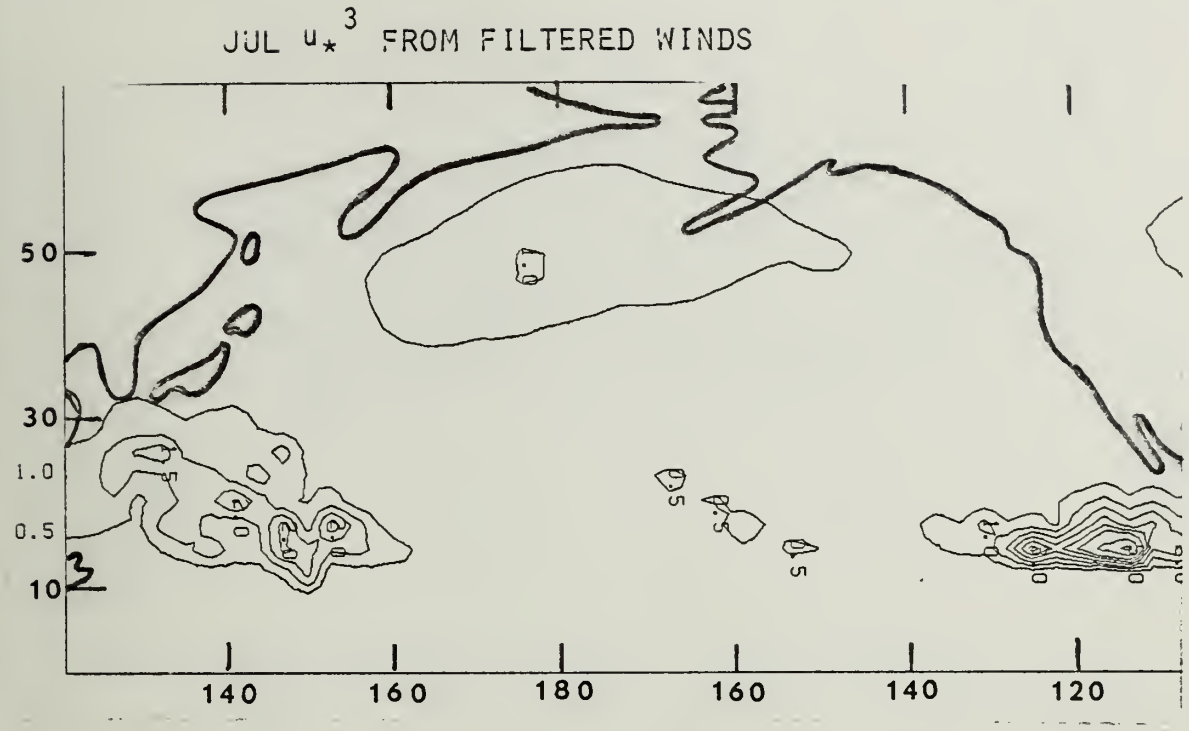

Figure 21. Same as Fig. 19 except for July.

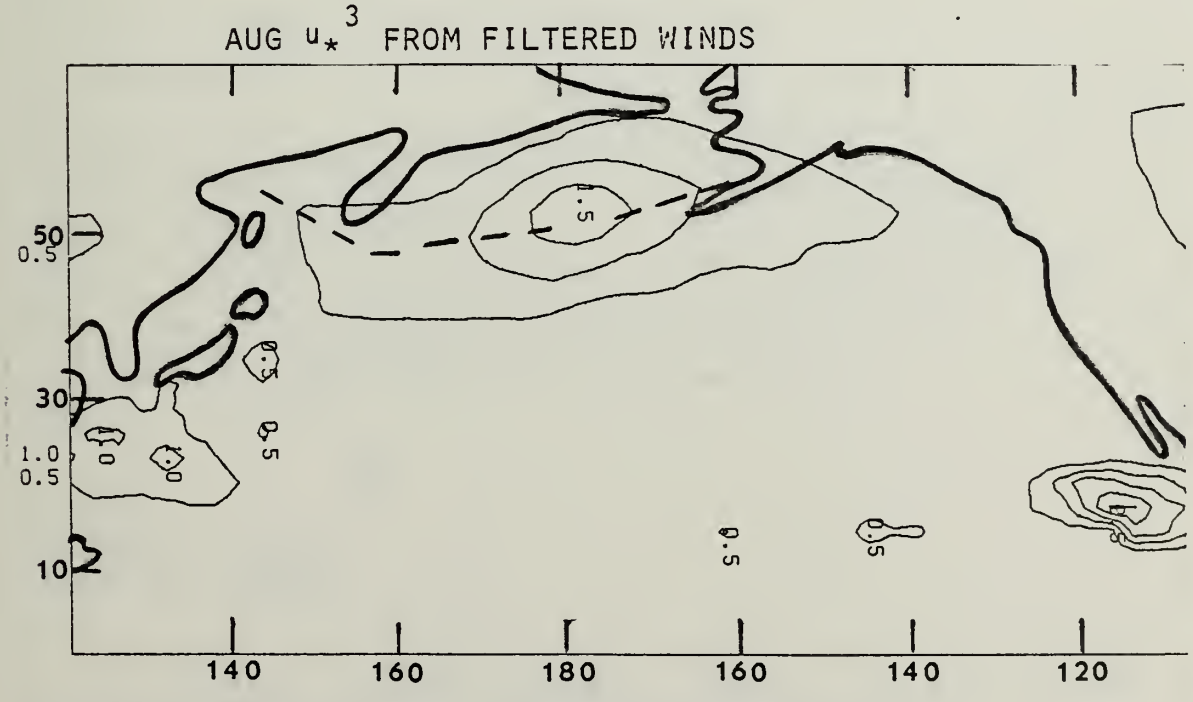

Figure 22. Same as Fig. 19 except for August.

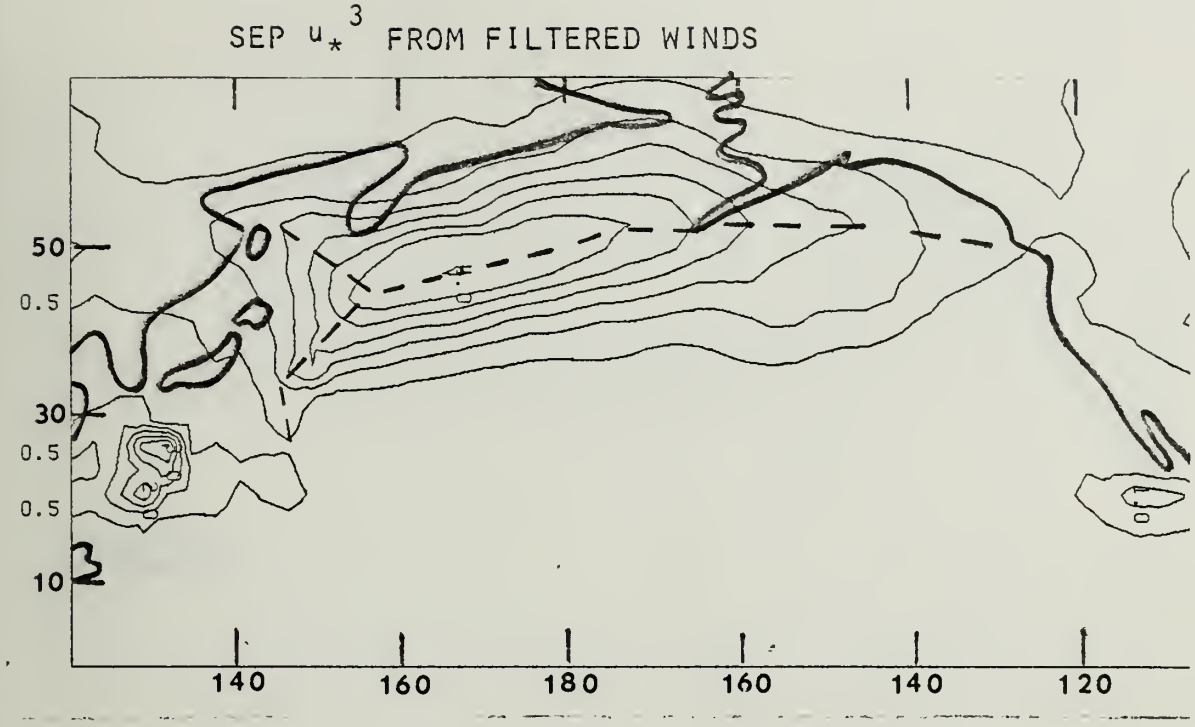

Figure 23. Same as Fig. 19 except for September.

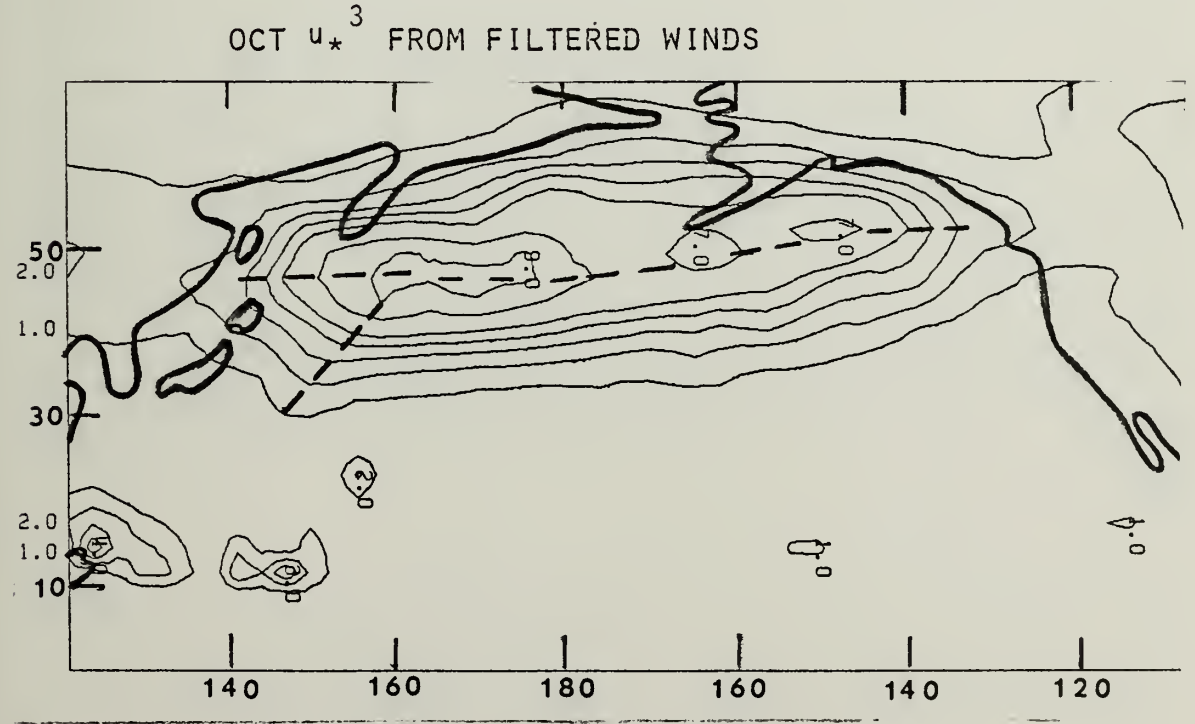

Figure 24. Same as Fig. 15 except for October.

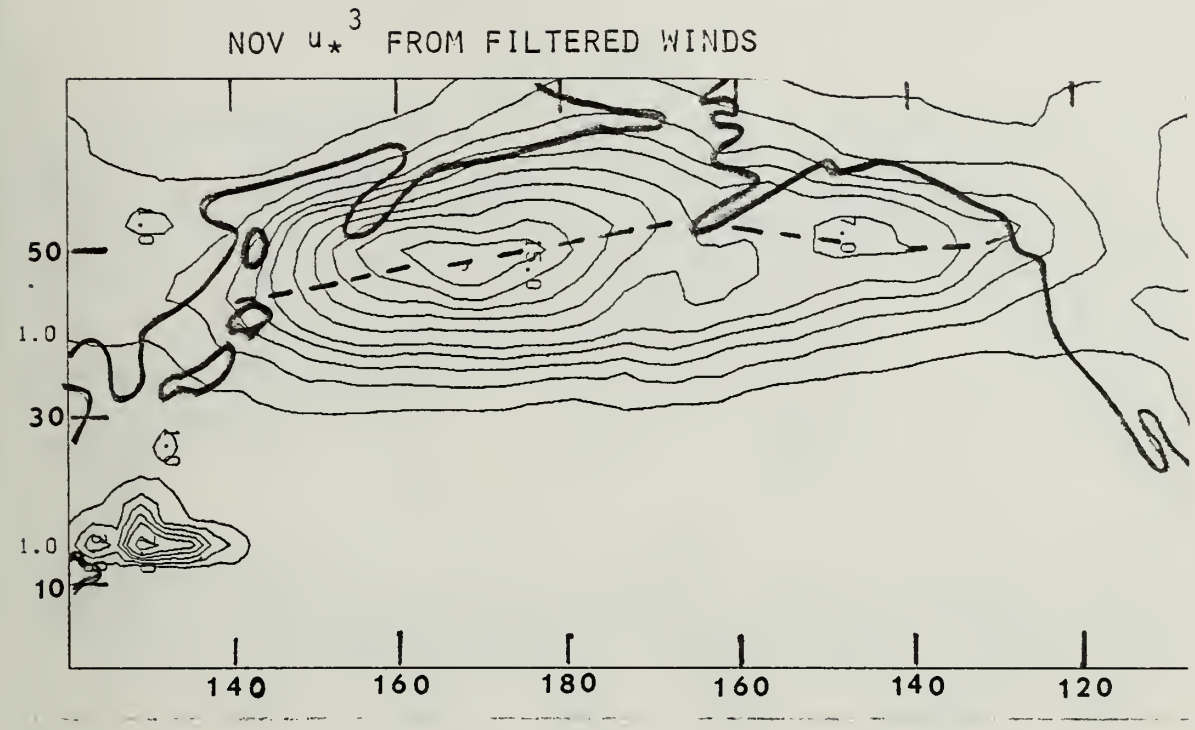

Figure 25. Same as Fig. 15 except for November.

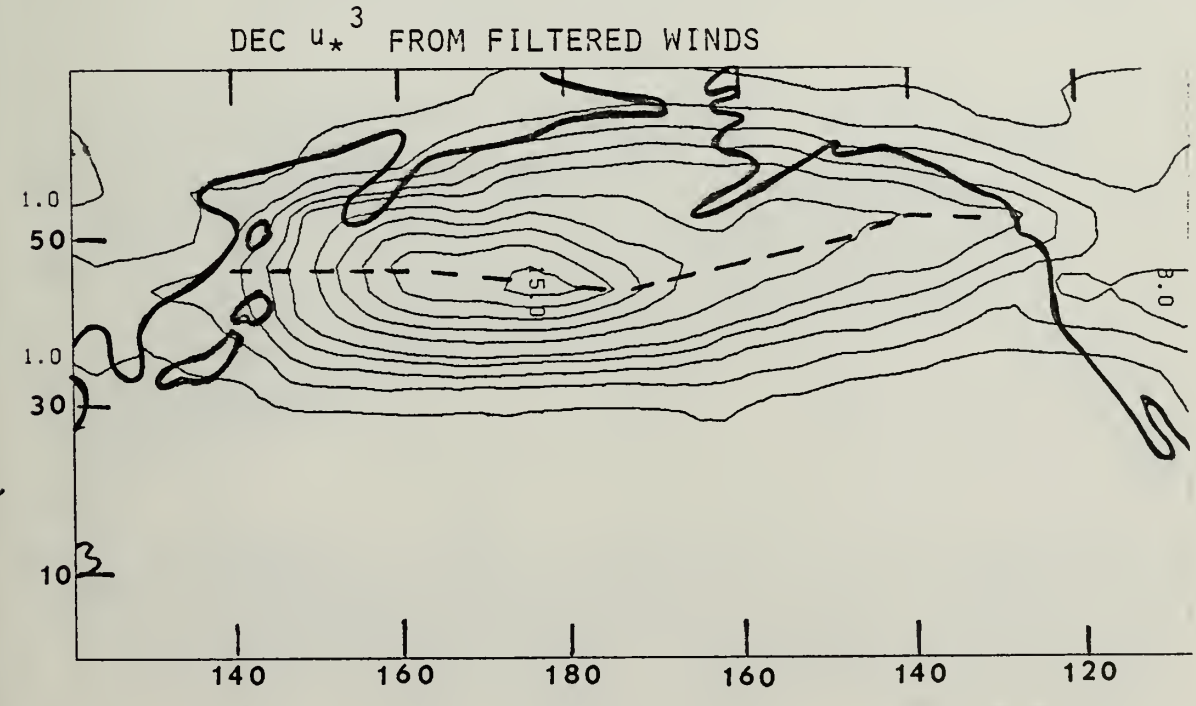

Figure 26. Same as Fig. 15 except for December.

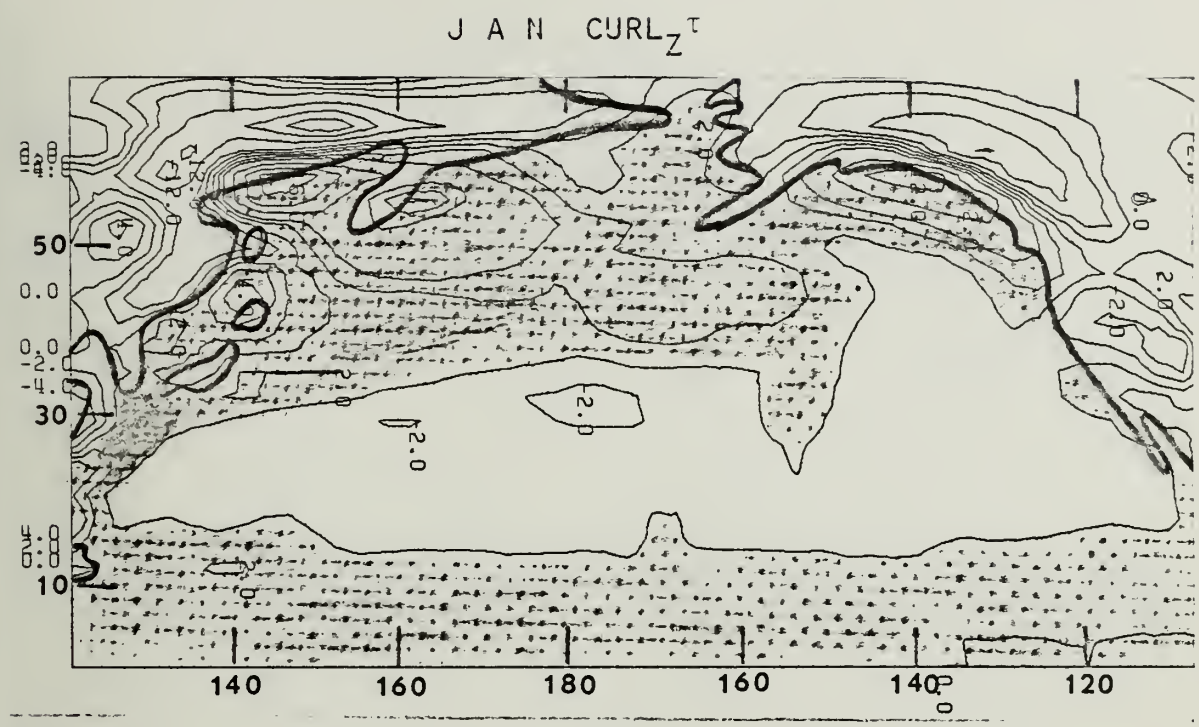

Figure 27. Climatological values of the vertical components of wind stress curl ($Curl_Z\tau$) from total u and v wind components. Contour values are -16.0,-12.0,-8.0,-4.0,-2.0,0.0,2.0,4.0, 8.0,12.0,16.0 x 10^{-8} dynes/cm^3. Shaded areas indicate positive curl.

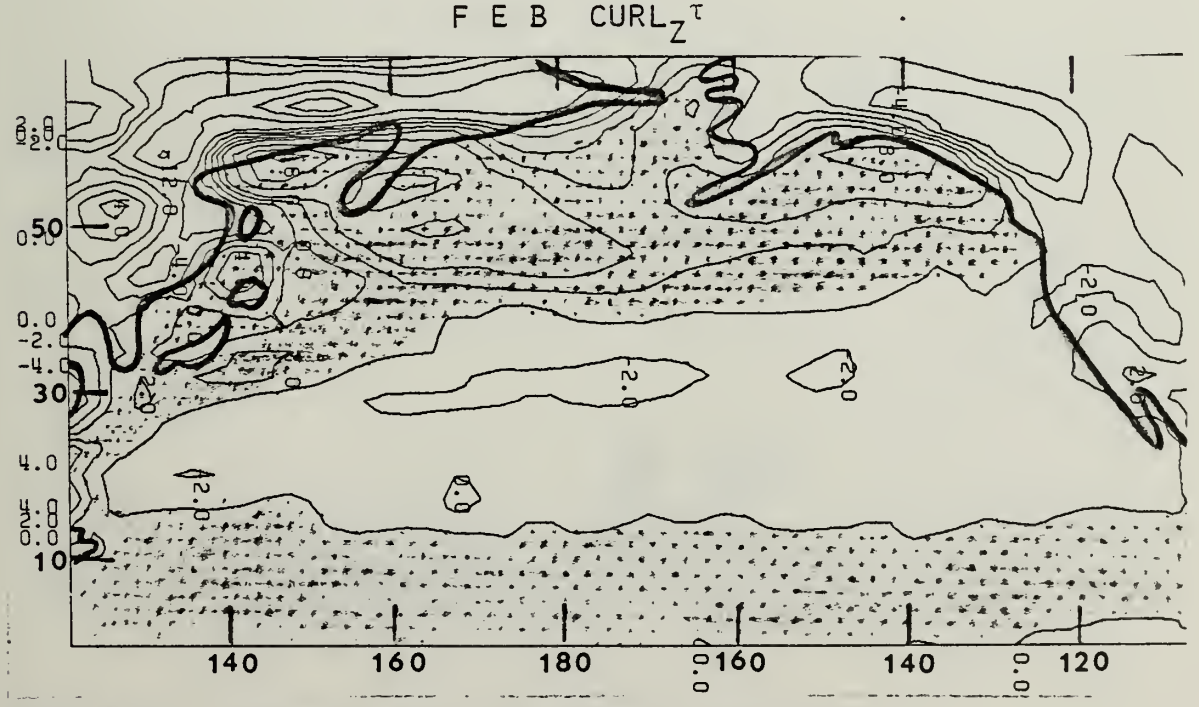

Figure 28. Same as Fig. 27 except for February.

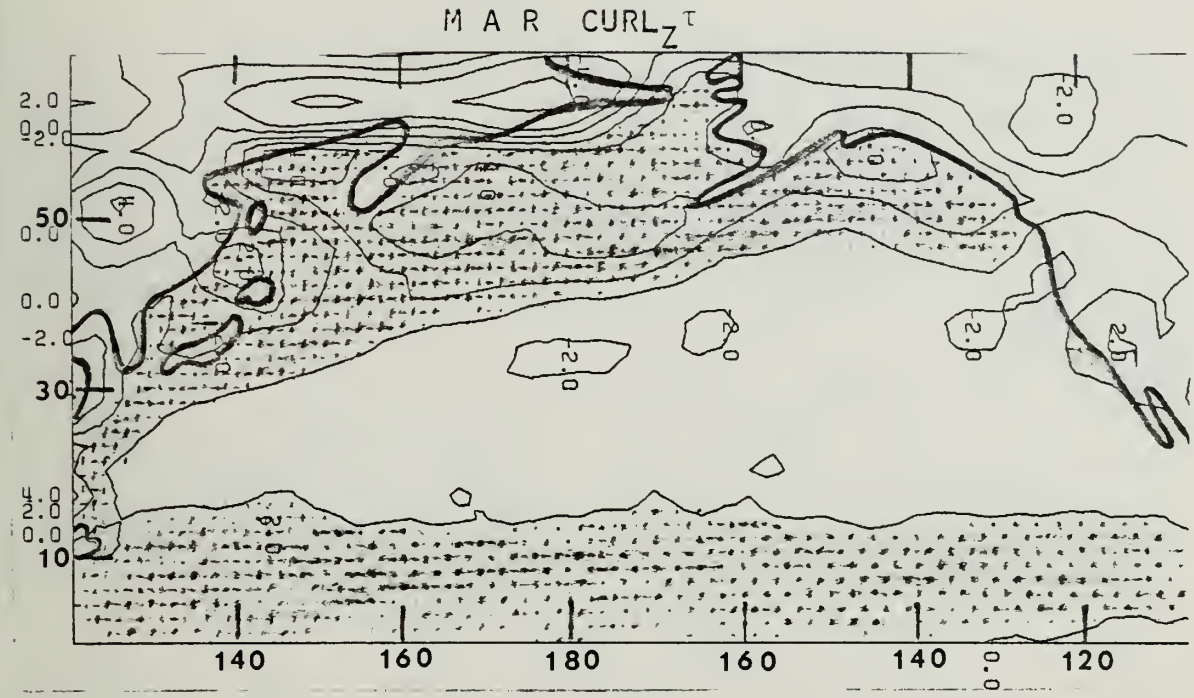

Figure 29. Same as Fig. 27 except for March.

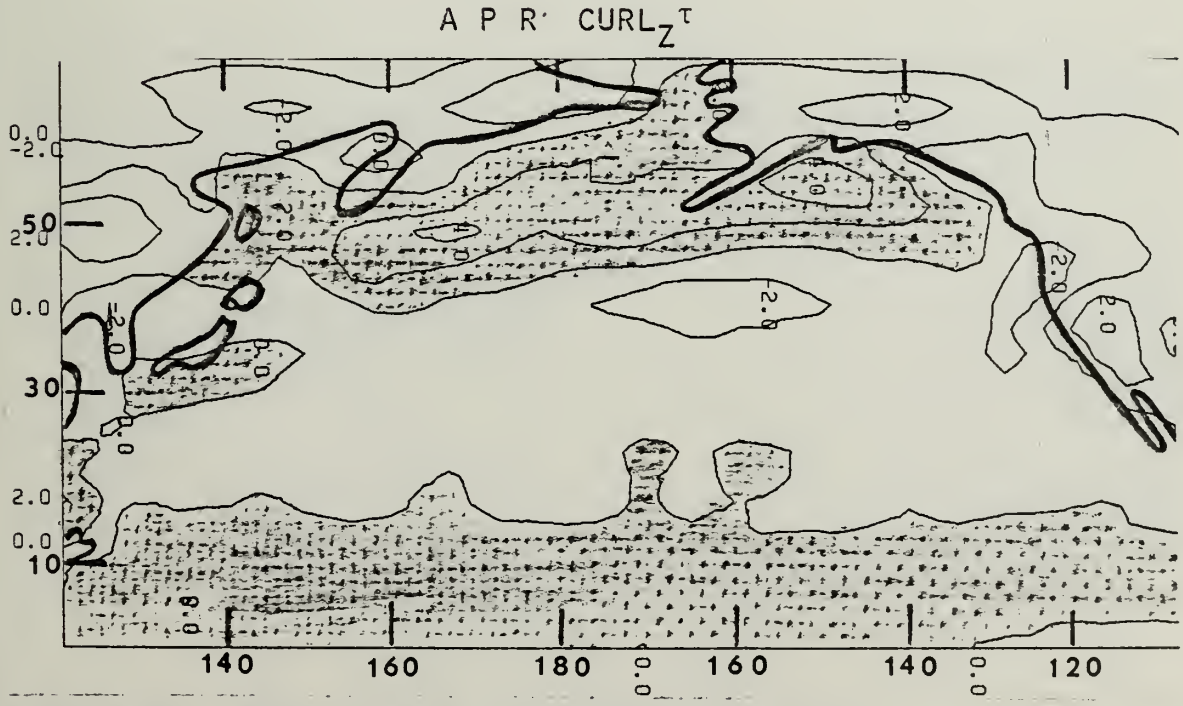

Figure 30. Same as Fig. 27 except for April.

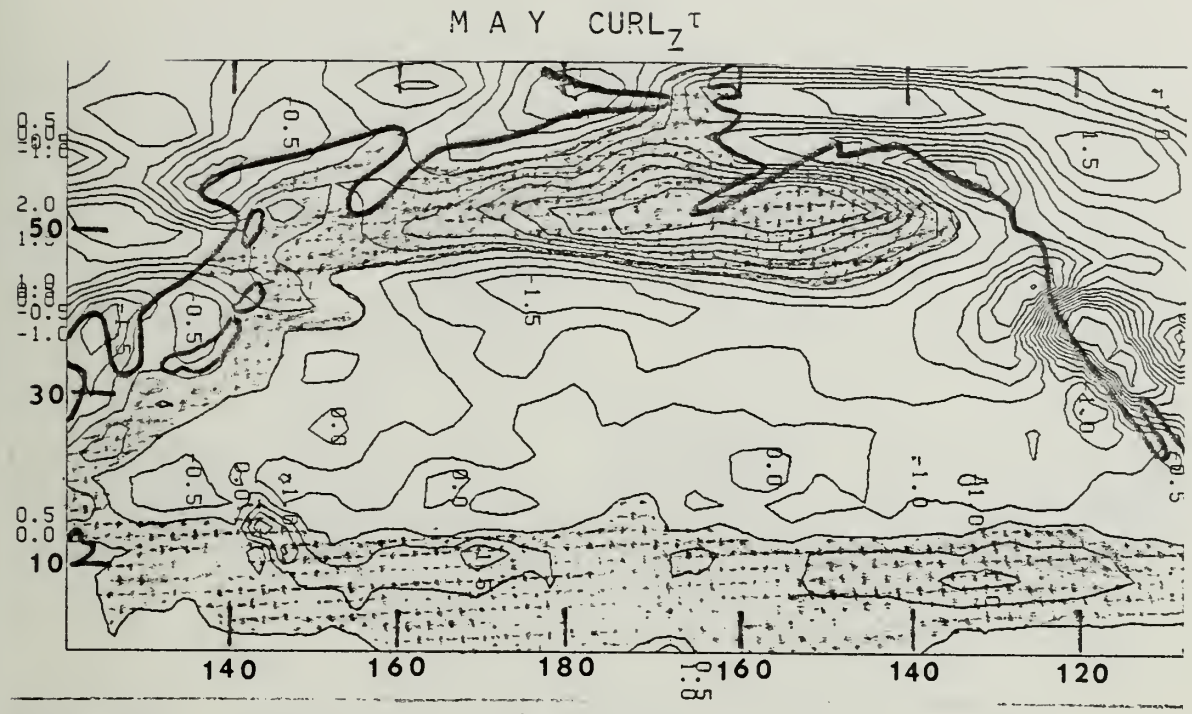

Figure 31. Same as Fig. 27 except contour values are -5.0,-4.0,-3.0,-2.5,-2.0,-1.5,-1.0,-0.5, 0.0,0.5,1.0,1.5,2.0,2.5,3.0,4.0,5.0 x 10^{-8} dynes/cm^3 and the month is May.

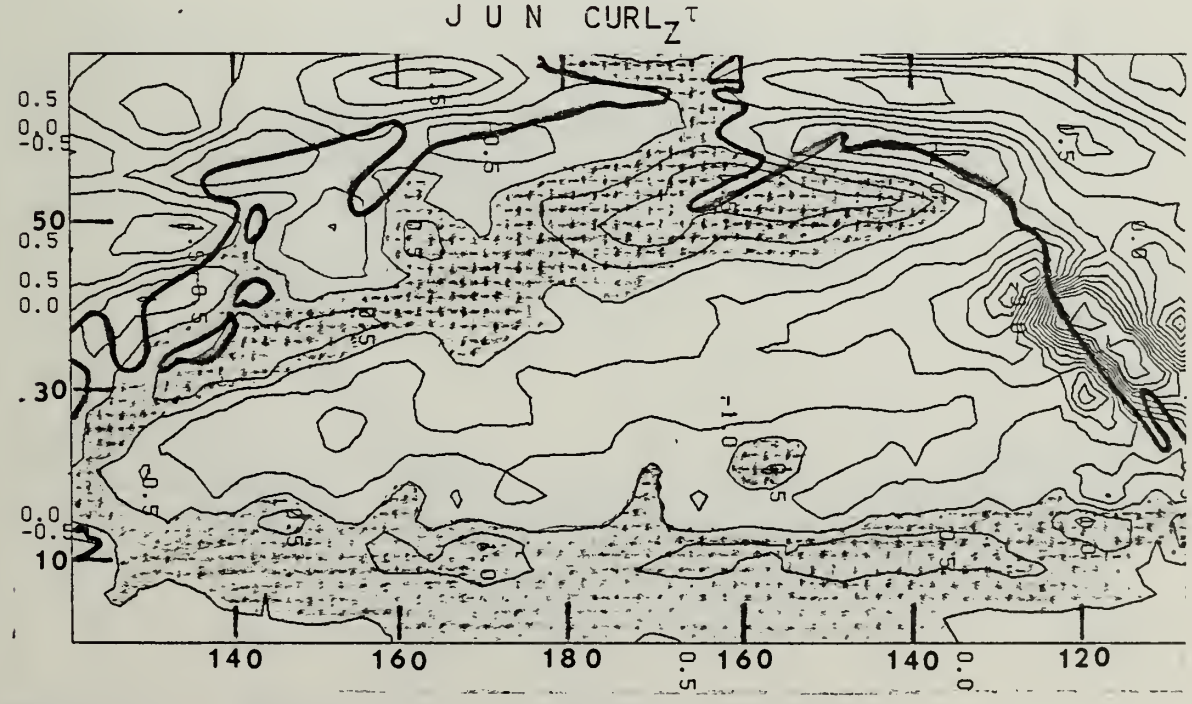

Figure 32. Same as Fig. 31 except for June.

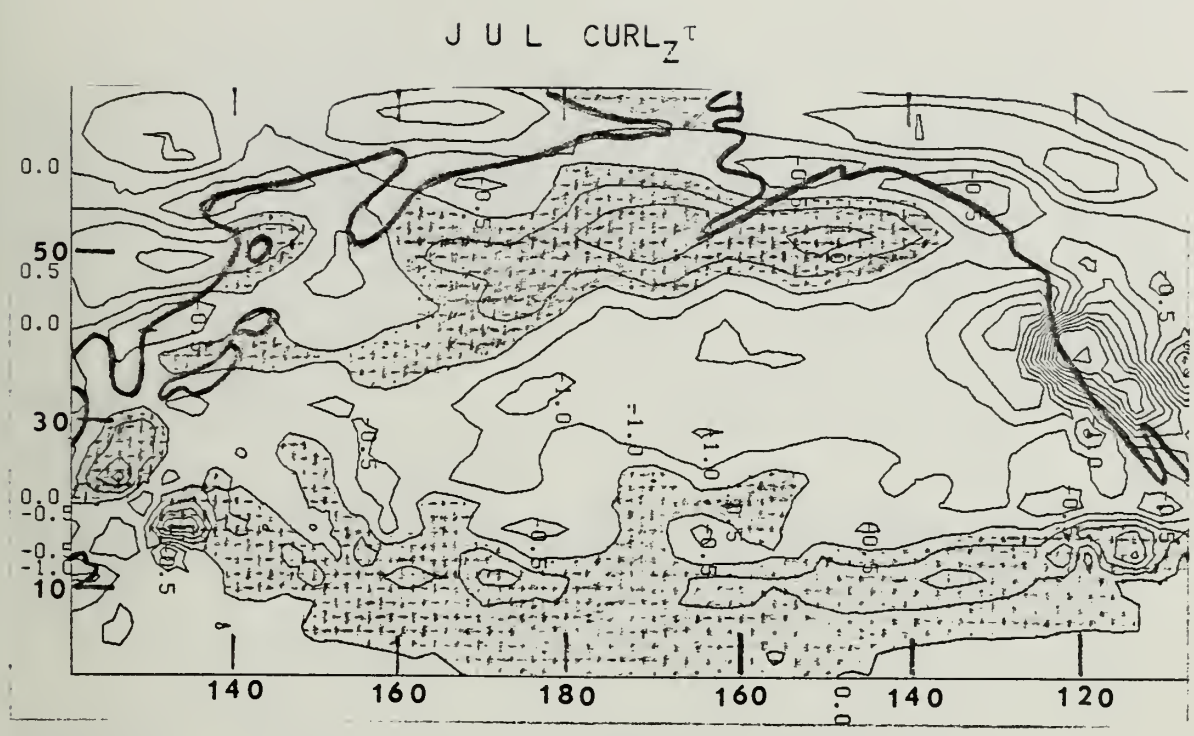

Figure 33. Same as Fig. 31 except for July.

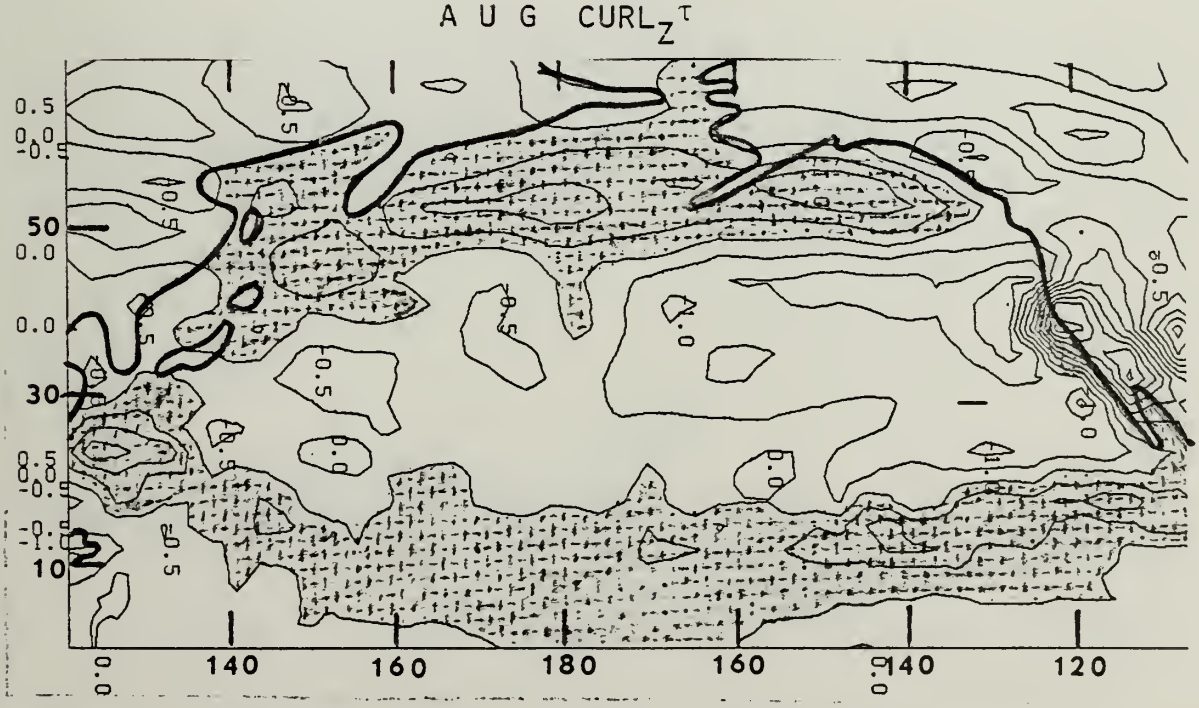

Figure 34. Same as Fig. 31 except for August.

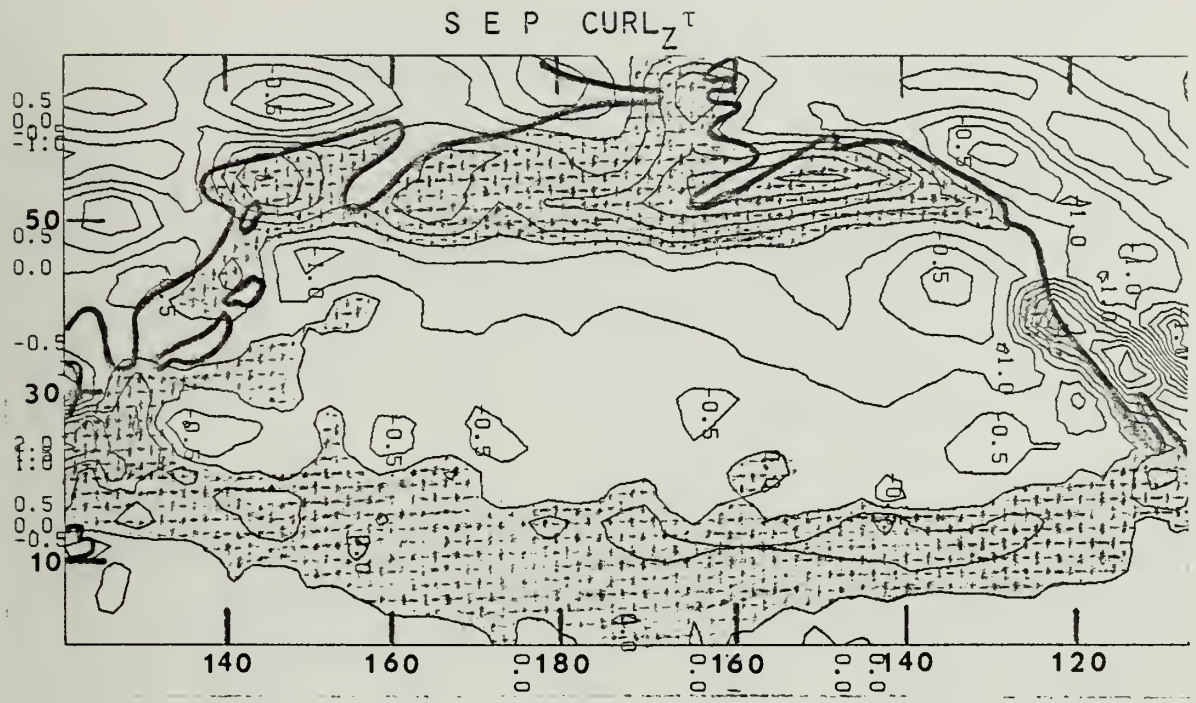

Figure 35. Same as Fig. 31 except for September.

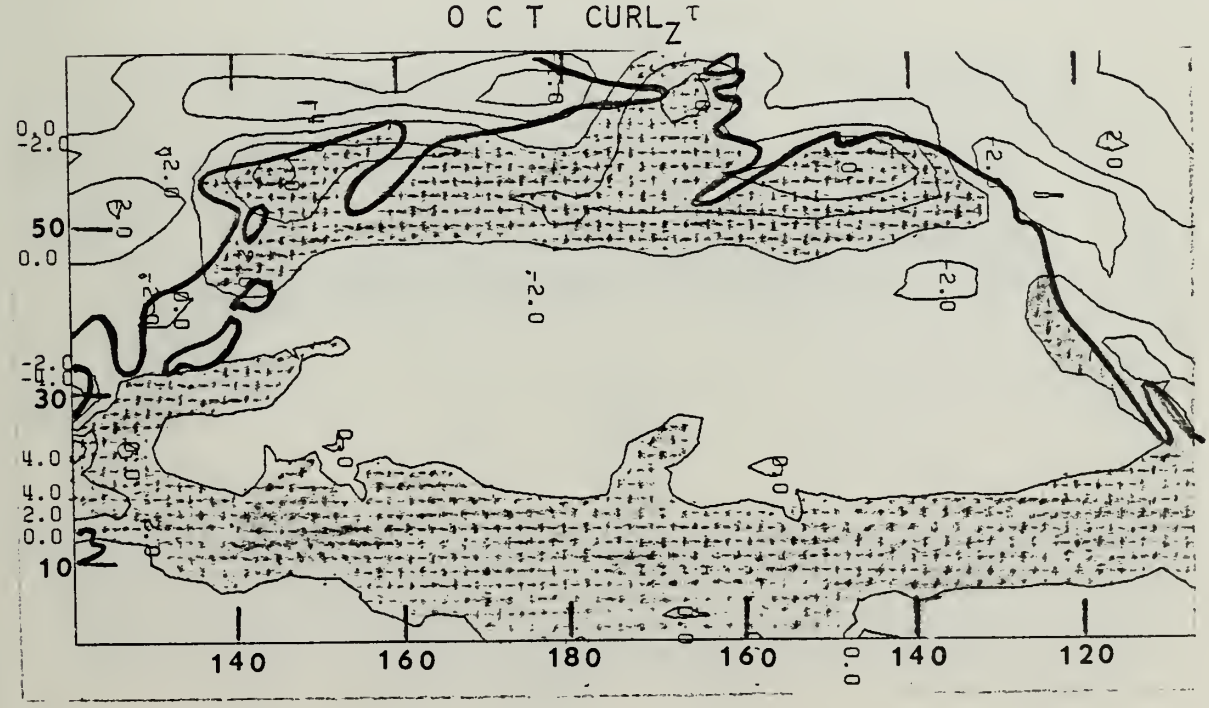

Figure 36. Same as Fig. 27 except for October.

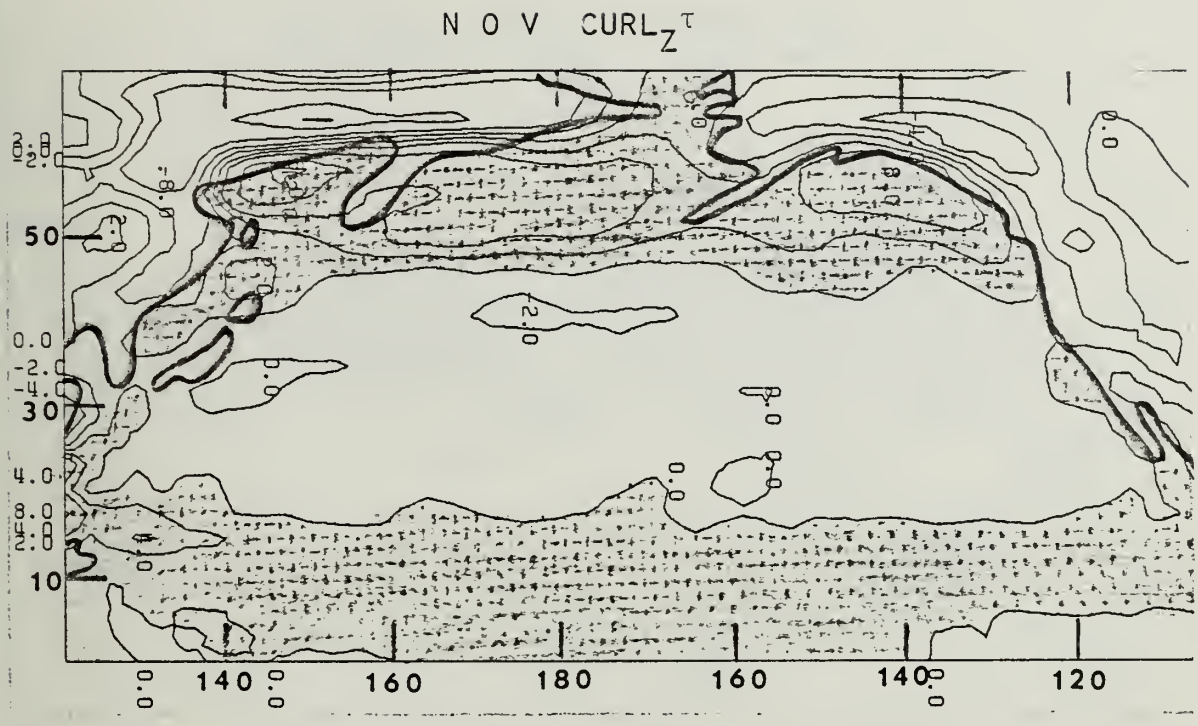

Figure 37. Same as Fig. 27 except for November.

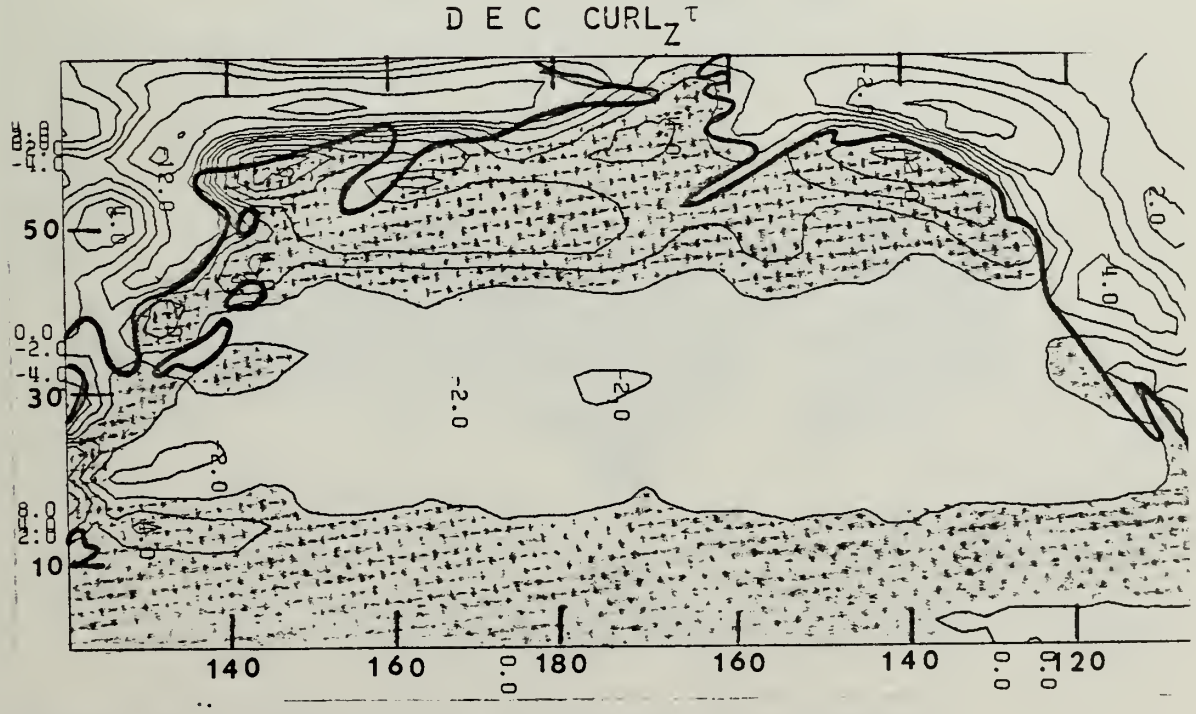

Figure 38. Same as Fig. 27 except for December.

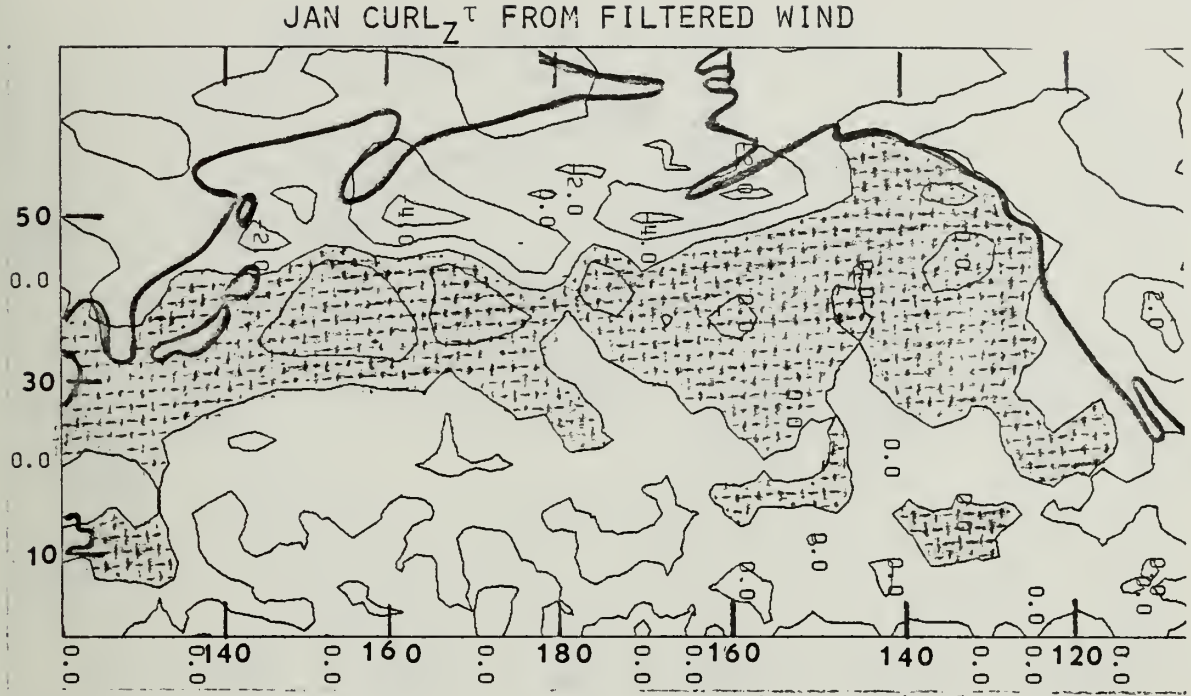

Figure 39. Climatological values of the vertical components of wind stress curl ($Curl_z\tau$) from high-pass filtered u and v wind components. Contour values are -4.0,-2.0,0.0,2.0,4.0 x 10^{-9} dynes/cm^3. Shaded areas indicate positive curl.

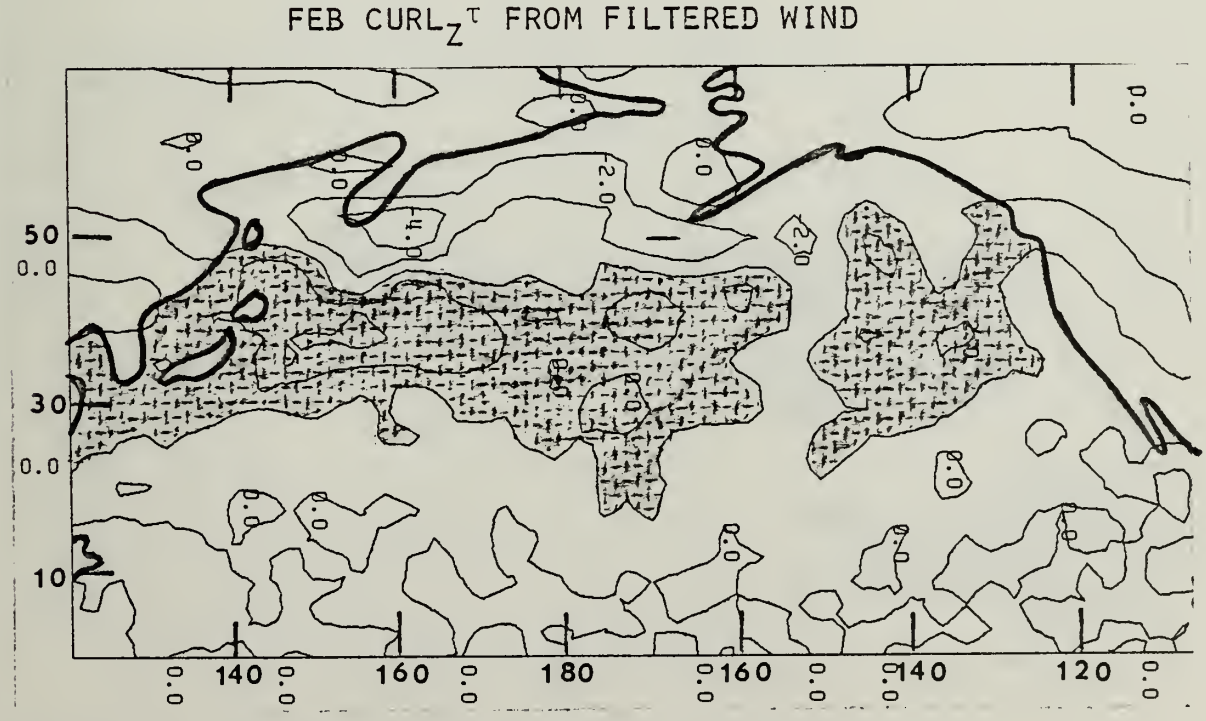

Figure 40. Same as Fig. 39 except for February.

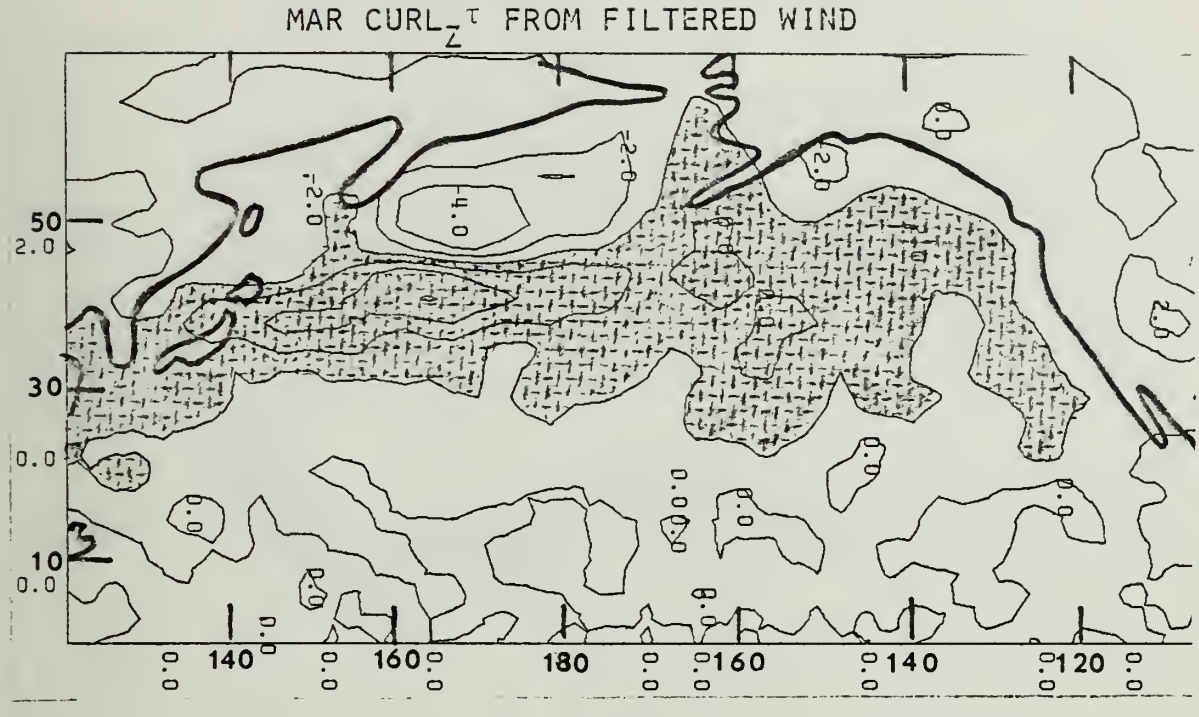

Figure 41. Same as Fig. 39 except for March.

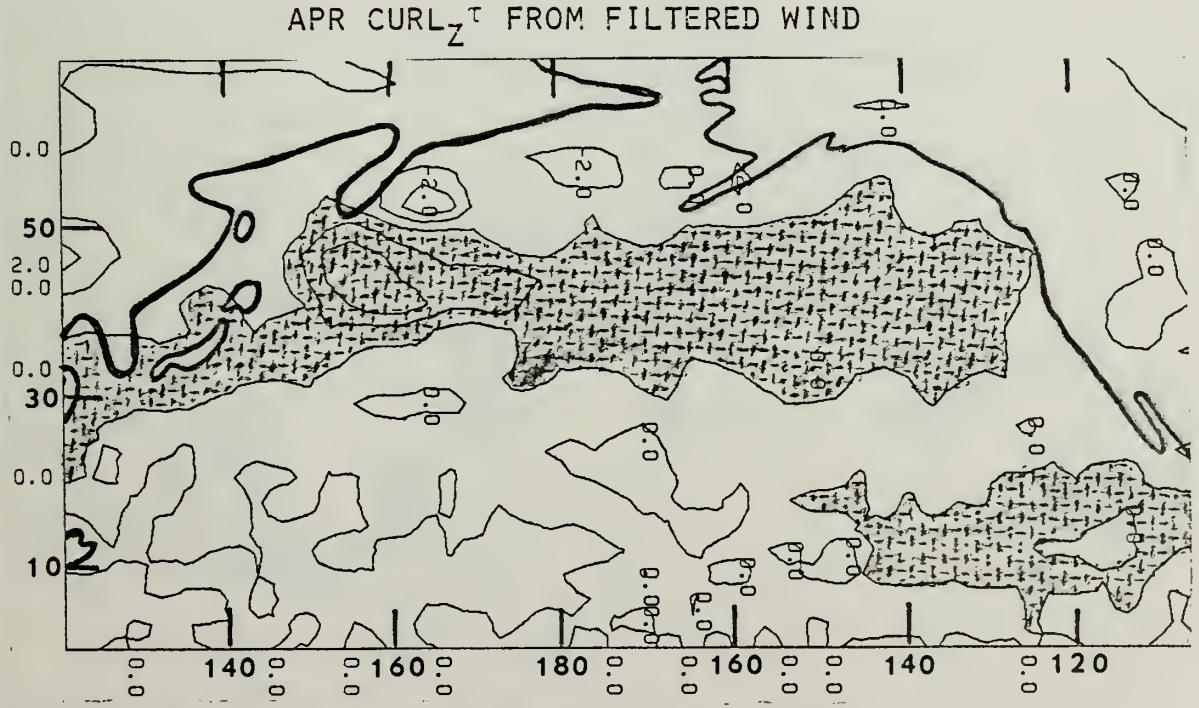

Figure 42. Same as Fig. 39 except for April.

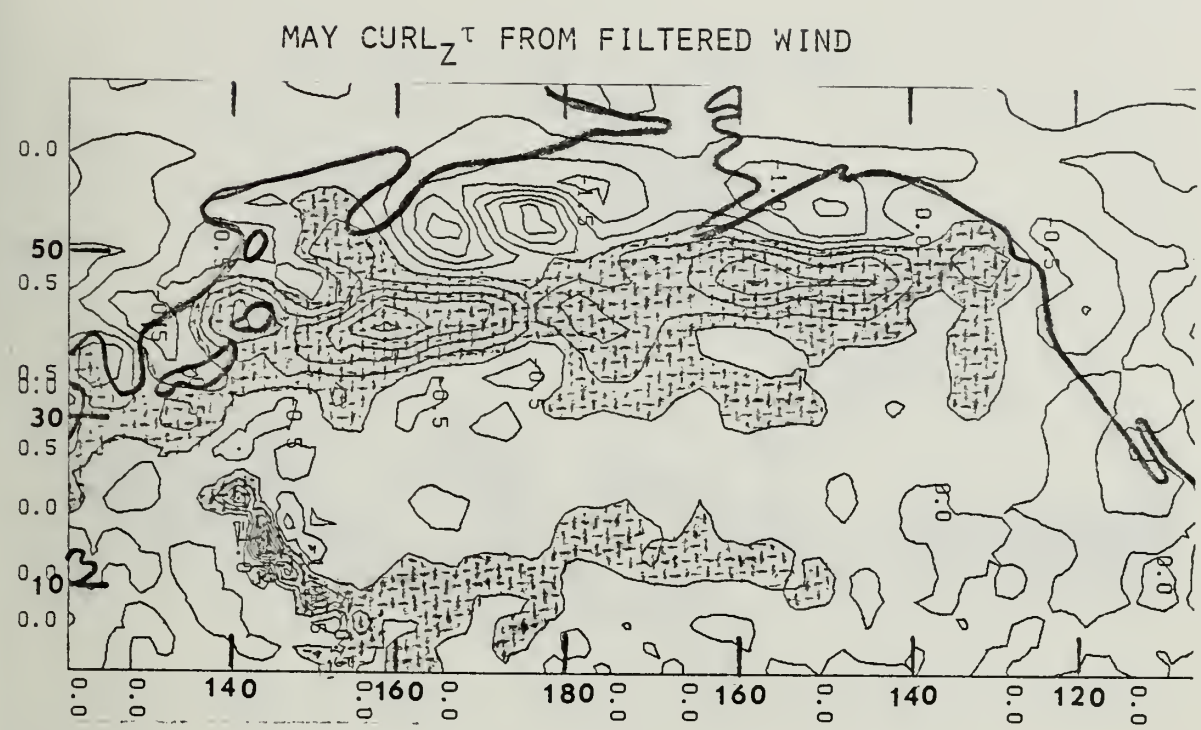

Figure 43. Same as Fig. 39 except contour values are -4.0,-3.5,-3.0,-2.5,-2.0,-1.5,-1.0,-0.5, 0.0,0.5,1.0,1.5,2.0,2.5,3.0,3.5,4.0 x 10^{-9} dynes/cm^3 and the month is May.

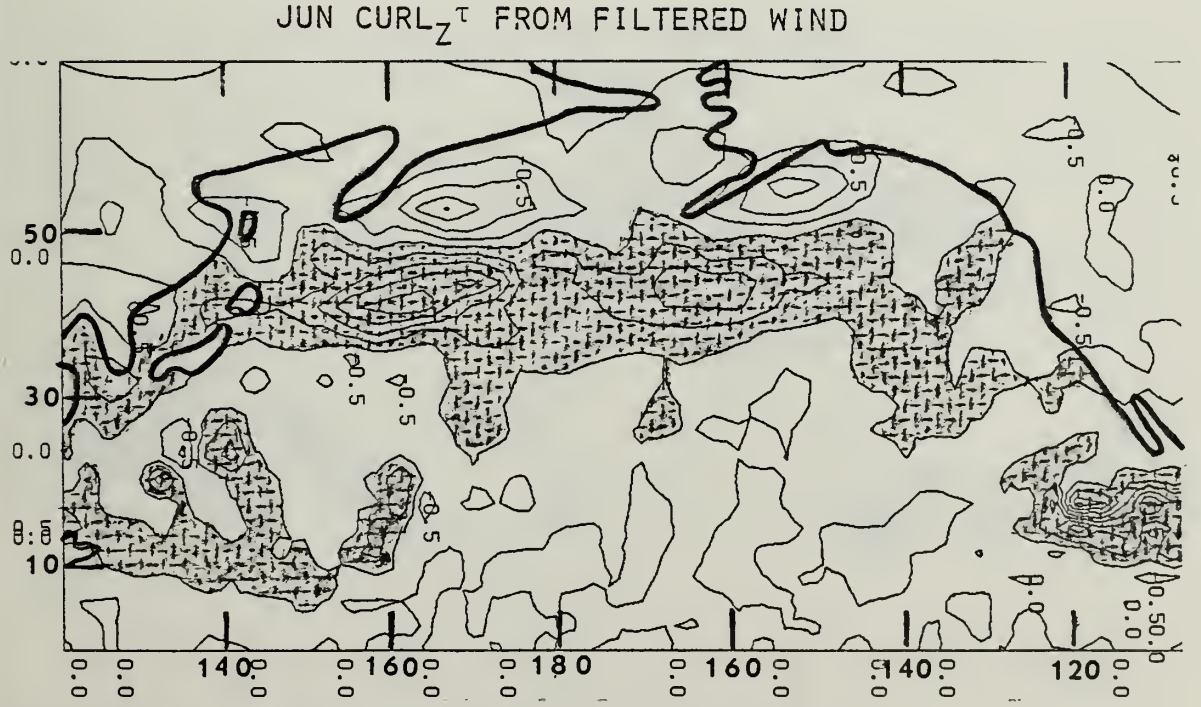

Figure 44. Same as Fig. 43 except for June.

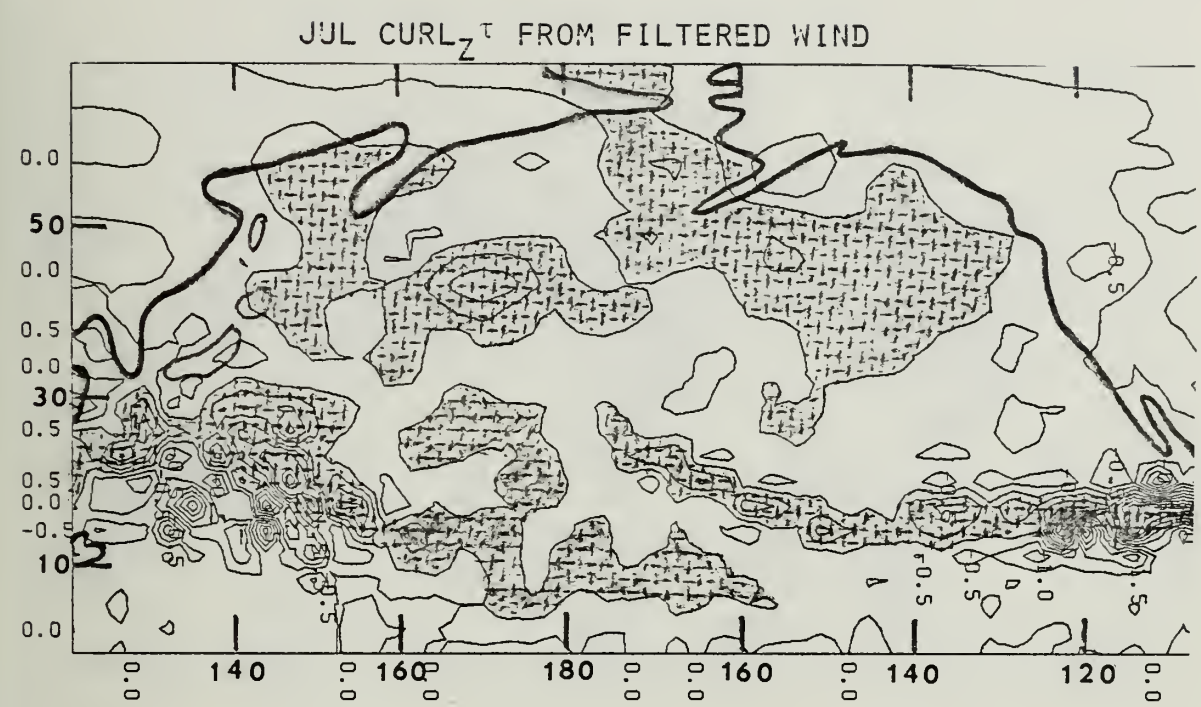

Figure 45. Same as Fig. 43 except for July.

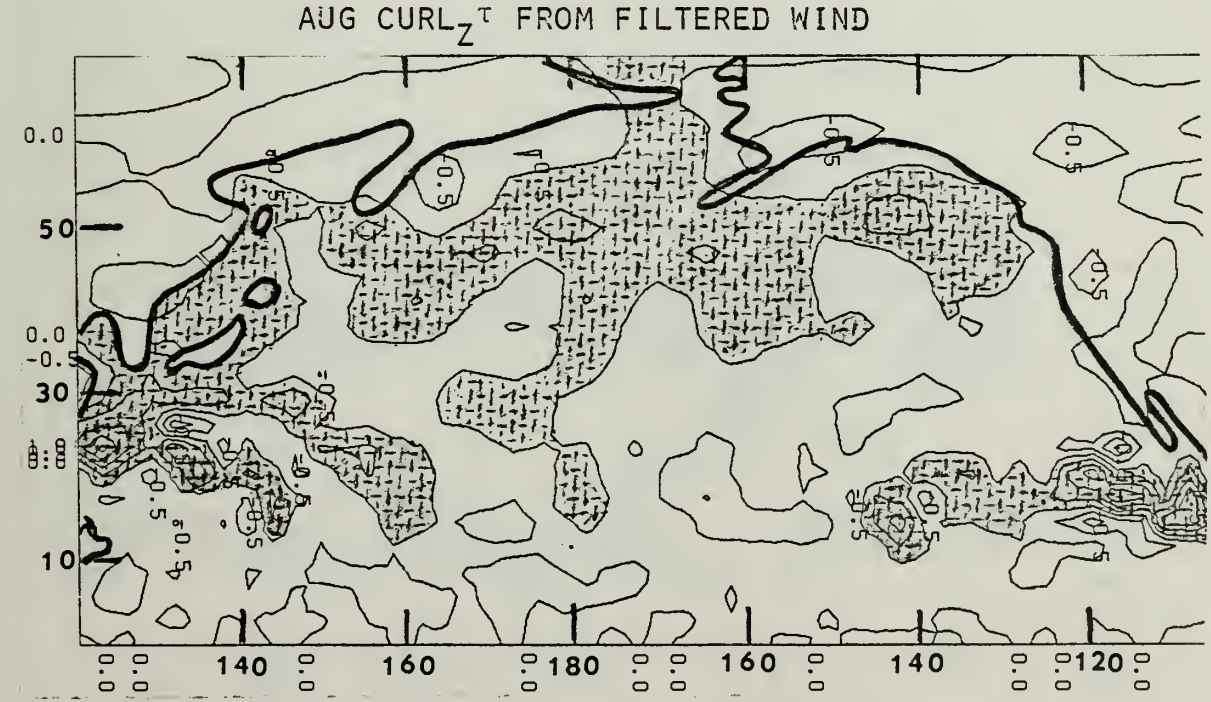

Figure 46. Same as Fig. 43 except for August.

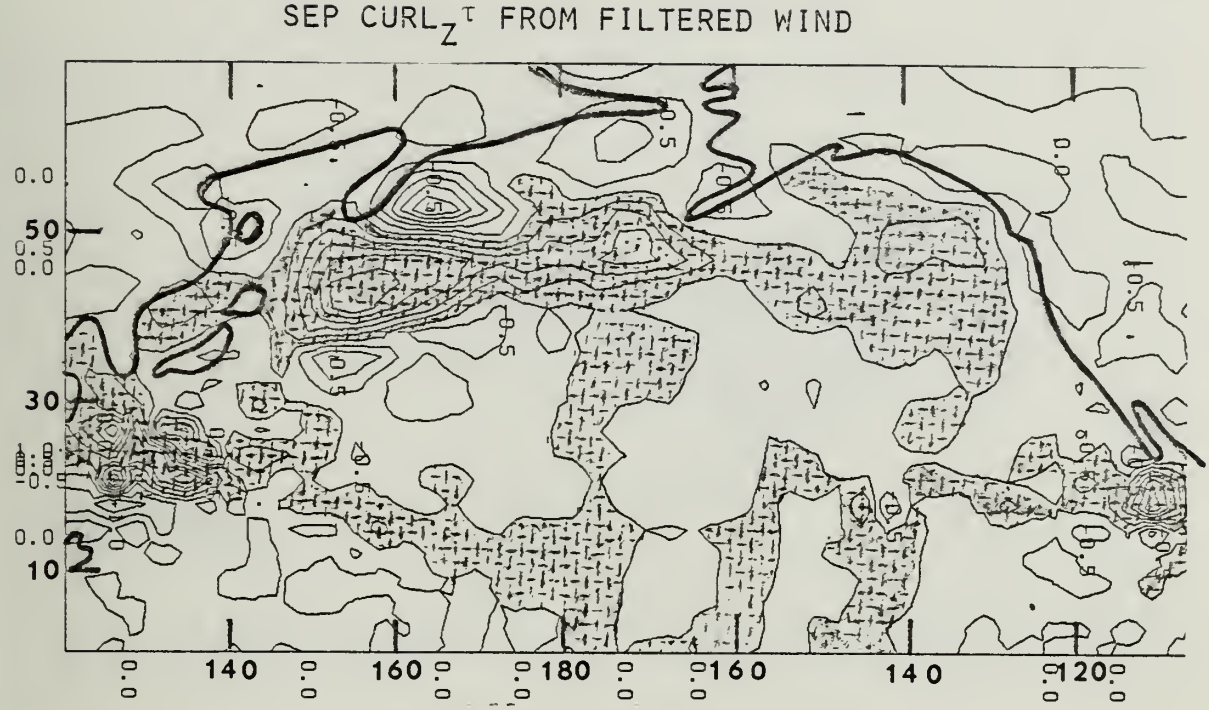

Figure 47. Same as Fig. 43 except for September.

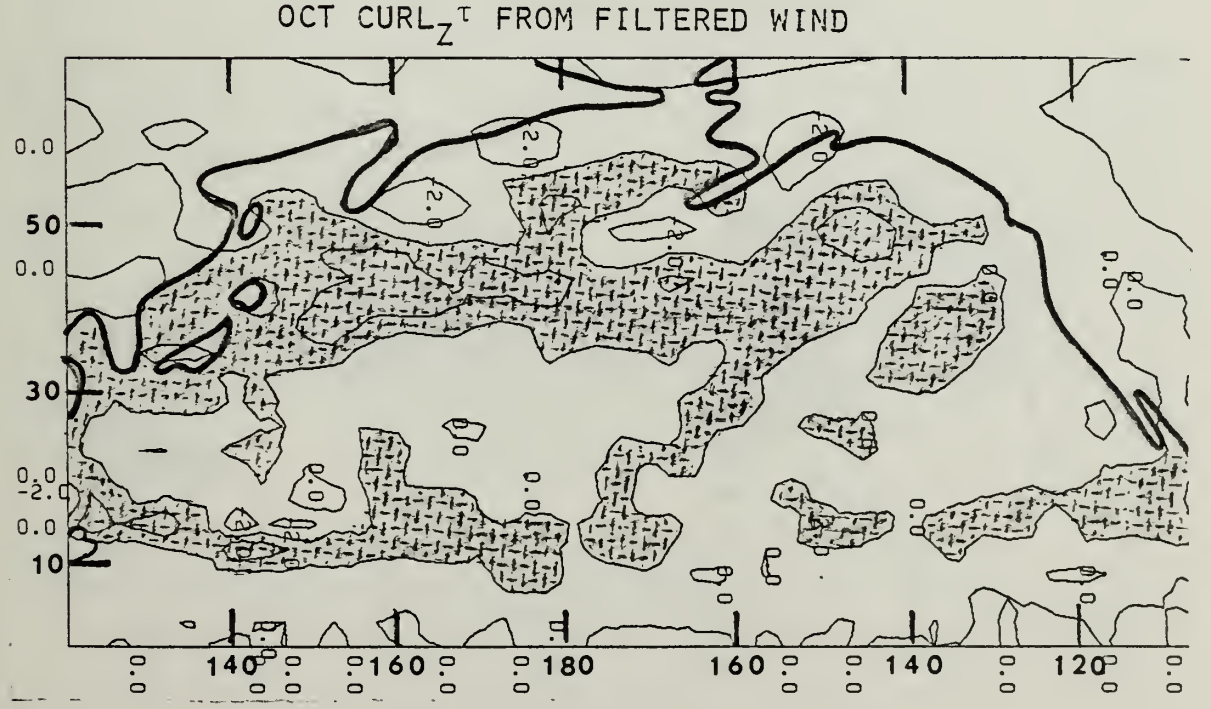

Figure 48. Same as Fig. 39 except for October.

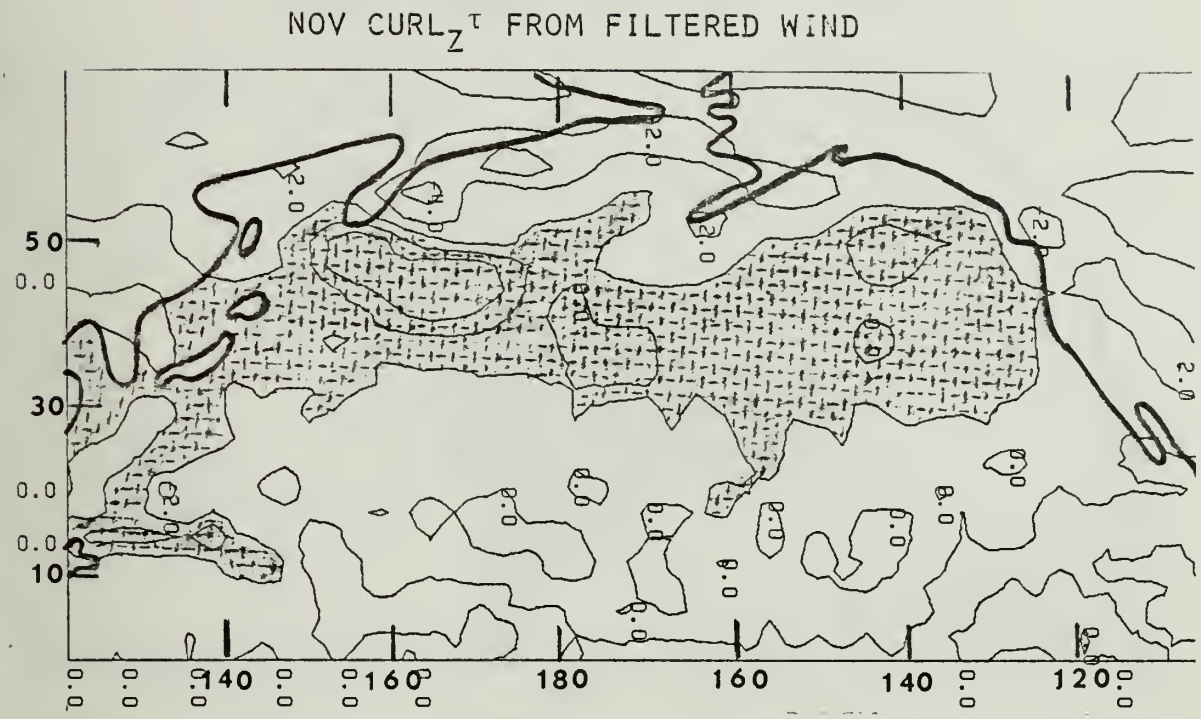

Figure 49. Same as Fig. 39 except for November.

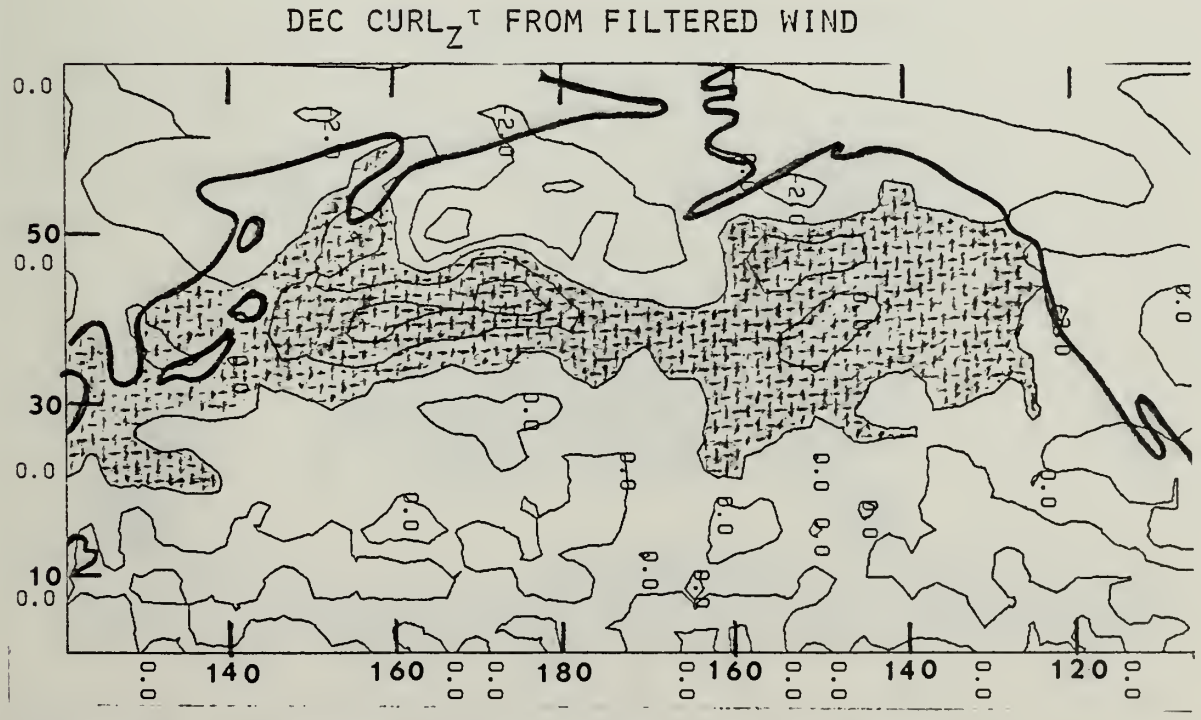

Figure 50. Same as Fig. 39 except for December.

SST ANOMALY CHANGE FROM SEP 76 TO MAR 77

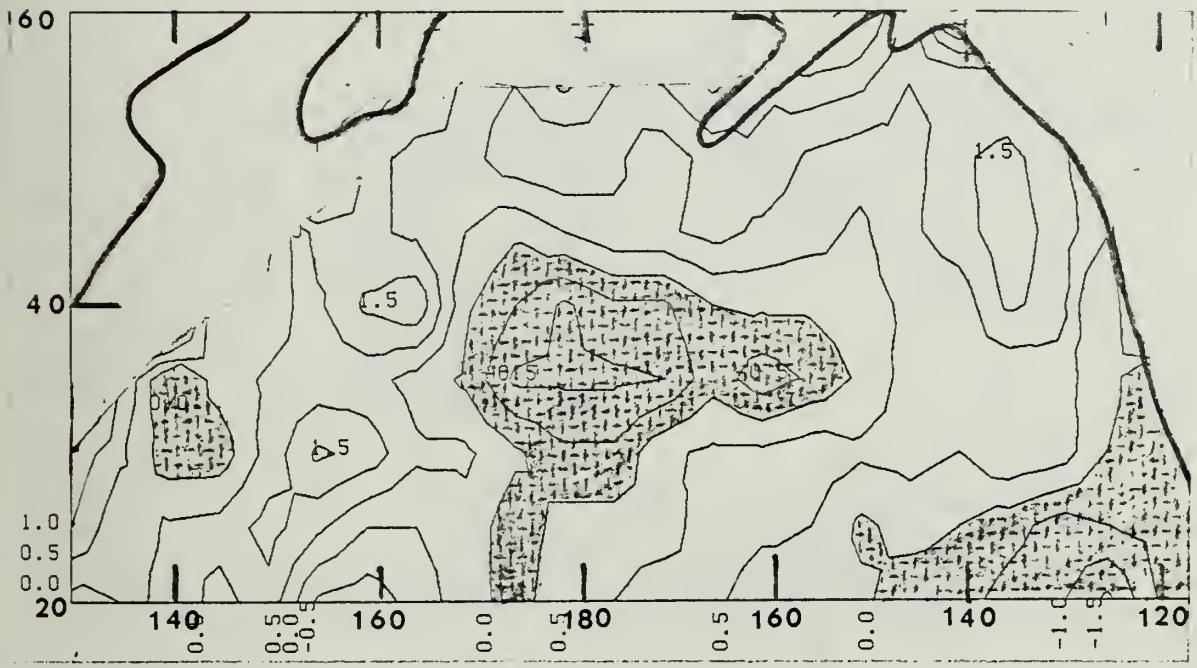

Figure 51. SST anomaly change from September 1976 to March 1977. Contour intervals are 0.5°C. Shaded areas indicate negative SST anomaly development.

u_*^3 ANOMALIES FOR SEP 76 TO MAR 77

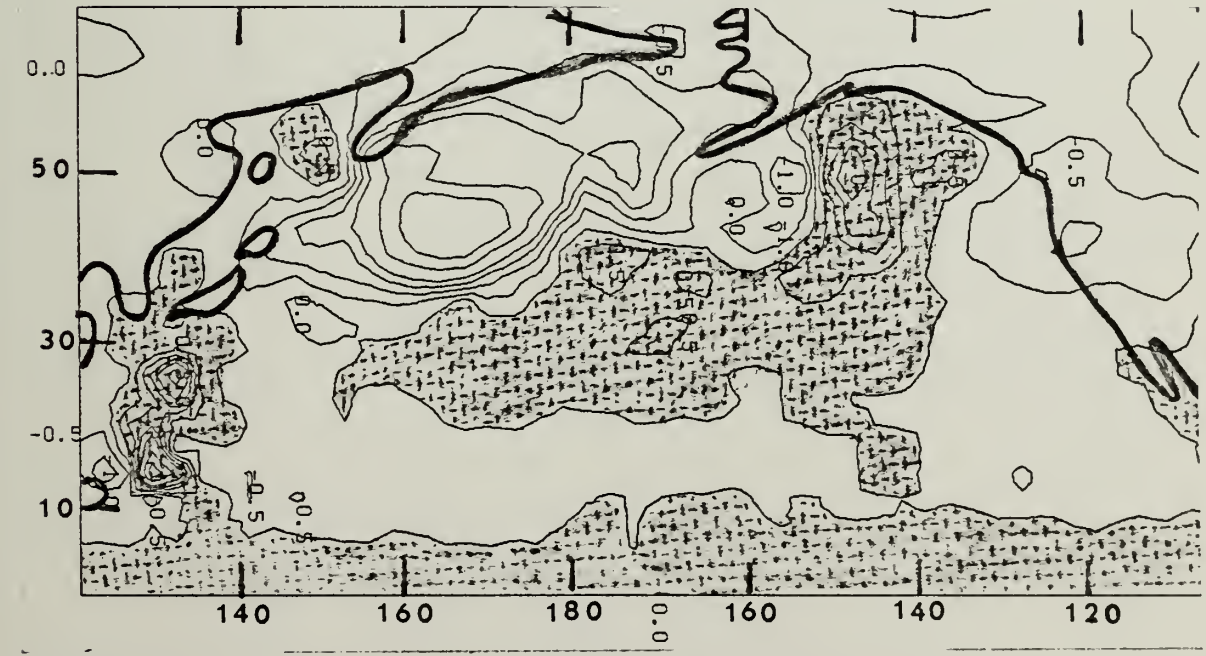

Figure 52. Filtered u_*^3 anomalies averaged from mid-September 1976 to mid-March 1977. Contour intervals are 0.5×10^4 $(cm/sec)^3$. Shaded areas indicate above normal storminess.

CURL$_Z{}^\tau$ ANOMALIES FOR SEP 76 TO MAR 77

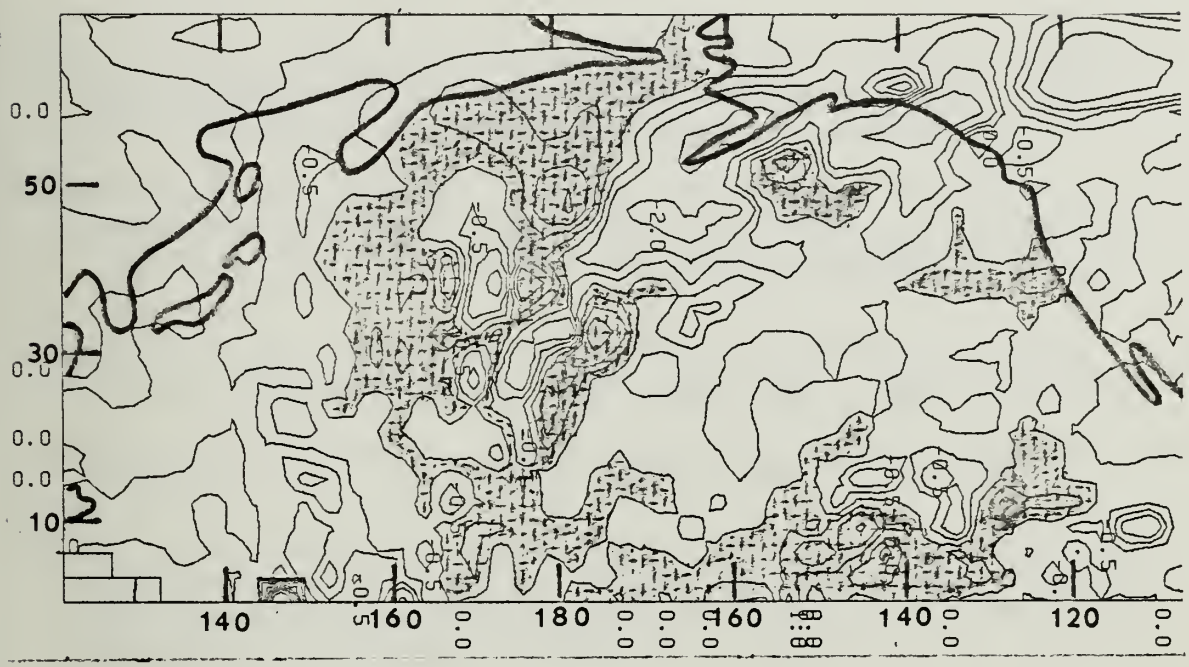

Figure 53. Filtered curl$_Z\tau$ anomalies averaged over the period mid-September 1976 to mid-March 1977. Contour intervals are 0.5 x 10^{-9} dynes/cm^3. Shaded areas indicate above normal curl$_Z\tau$ values.

LIST OF REFERENCES

Davis, R. E., 1976: Predictability of sea surface temperature and sea level pressure anomalies over the North Pacific Ocean. J. Phys. Oceanogr., 6, 249-266.

Elsberry, R. L., and N. T. Camp, 1978: Oceanic thermal response to strong atmospheric forcing. I. Characteristics of forcing events. J. Phys. Oceanogr., 8, 206-214.

Garratt, J. R., 1977: Review of drag coefficients over oceans and continents. Mon. Wea. Rev., 105, 915-929.

Haltiner, G. J., 1971: Numerical Weather Prediction, Wiley, 317 pp.

Heise, G. C., 1977: A statistical study of synoptic storm activity over the North Pacific in 1975. M.S. Thesis, Department of Meteorology, Naval Postgraduate School, Monterey, California, 51 pp.

Lazanoff, S. M., and N. M. Stevenson, 1978: A twenty-year Northern Hemisphere wave spectral climatology, in Turbulent Fluxes through the Sea Surface, Wave Dynamics, and Prediction, edited by A. Favre and K. Hasselmann, Plenum, 547-564.

Mendenhall, B. R., M. M. Holl, and M. J. Cumming, 1978: Development of a marine history of analyzed sea-level pressure fields and diagnosed wind fields. Fleet Numerical Oceanographic Center, Monterey, California, Tech. Rep. M-227, 41 pp. [DDC Number AD A075413].

Namias, J., 1972: Large scale and long term fluctuations in some atmospheric and oceanic variables, in Nobel Symposium 20, edited by D. Dyrssen and D. Jagner, Wiley, 27-48.

_____, 1978: Multiple causes of the North American abnormal winter 1976-77. Mon. Wea. Rev., 106, 279-295.

Saunders, P. M., 1976: On the uncertainty of wind stress curl. J. Mar. Res., 32, 155-160.

Simpson, J., 1969: On some aspects of sea-air interaction in middle latitudes. Deep Sea Res. Supplement, 16, 233-261.

White, W. B., and R. L. Haney, 1978: The dynamics of ocean climate variability. Oceanus, 21, 33-39.

INITIAL DISTRIBUTION LIST

		No. Copies
1.	Defense Technical Information Center Cameron Station Alexandria, Virginia 22314	2
2.	Library, Code 0142 Naval Postgraduate School Monterey, California 93940	2
3.	Commander Naval Oceanography Command NSTL Station, Mississippi 39529	1
4.	Commanding Officer Fleet Numerical Oceanography Center Monterey, California 93940	1
5.	Officer-in-Charge Naval Environmental Prediction Research Facility Monterey, California 93940	1
6.	Prof. G. J. Haltiner, Code 63Ha Naval Postgraduate School Monterey, California 93940	1
7.	Prof. C.N.K. Mooers, Code 68Mr Naval Postgraduate School Monterey, California 93940	1
8.	Prof. R. L. Elsberry, Code 63Es Naval Postgraduate School Monterey, California 93940	1
9.	Department of Meteorology Library, Code 63 Naval Postgraduate School Monterey, California 93940	1
10.	Dr. Manfred M. Holl Meteorology International, Inc. 2600 Garden Road, Suite 145 Monterey, California 93940	1
11.	Prof. R. L. Haney, Code 63Hy Naval Postgraduate School Monterey, California 93940	2
12.	Dr. Steve Pazan (NORPAX A-030) Scripps Institution of Oceanography La Jolla, California 92093	1

13. Dr. Don Gillman — 1
National Meteorological Center
National Weather Service, NOAA
Washington, D.C. 20233

14. Capt. Gary C. Heise — 1
12905 South 31st Street
Omaha, Nebraska 68123

15. Prof. J. M. Wallace — 1
Dept. of Atmospheric Sciences
University of Washington
Seattle, Washington 98195

16. Dr. M. Miyake — 1
IOS
9860 W. Saanich Rd.
P.O. Box 5000
Sidney, B.C. V8L 4B2
Canada

17. Wayne L. Darnell (M.S. 271) — 1
NASA, Langley Research Center
Hampton, Virginia 23665

18. Dr. David Halpern — 1
Pacific Marine Environmental Lab.
3711 15th Ave. NE
Seattle, Washington 98105

19. Capt. William J. Kaveney — 1
AFIT/CIRF
Wright-Patterson AFB, Ohio 45433

20. HQ Air Weather Service — 1
Technical Library
Scott AFB, Illinois 62225

21. Capt. Scott Risch — 2
Det 1, 1WW
COMNAVMARIANAS Box 17
FPO San Francisco 96630

Thesis
R5767 Risch
c.1
189386
A climatological study of the forcing of the North Pacific Ocean by synoptic storm activity.